Stapp Car Crash Journal, Vol. 60 (November 2016), pp.

The Large Omnidirectional Child (LODC) ATD: Biofidelity Comparison with the Hybrid III 10 Year Old

Jason Stammen, Kevin Moorhouse
National Highway Traffic Safety Administration

Brian Suntay
Transportation Research Center Inc.

Michael Carlson, Yun-Seok Kang
The Ohio State University

ABSTRACT – When the Hybrid III 10-year old (HIII-10C) anthropomorphic test device (ATD) was adopted into Code of Federal Regulations (CFR) 49 Part 572 as the best available tool for evaluating large belt-positioning booster seats in Federal Motor Vehicle Safety Standard (FMVSS) No. 213, NHTSA stated that research activities would continue to improve the performance of the HIII-10C to address biofidelity concerns. A significant part of this effort has been NHTSA's in-house development of the Large Omnidirectional Child (LODC) ATD. This prototype ATD is comprised of (1) a head with pediatric mass properties, (2) a neck that produces head lag with Z-axis rotation at the atlanto-occipital joint, (3) a flexible thoracic spine, (4) multi-point thoracic deflection measurement capability, (5) skeletal anthropometry representative of a seated child, and (6) an abdomen that can directly measure belt loading. The objective of this study was to evaluate the LODC by comparing its body region and full-body responses to both standard HIII-10C responses and pediatric biomechanical data. In body region tests, the LODC (BioRank = 1.21) showed improved biofidelity over the HIII-10C (BioRank = 2.70). The LODC also exhibited kinematics more similar to pediatric PMHS kinematics in a reconstruction test. In FMVSS No. 213 tests, the LODC was observed to have lower HIC values with the absence of hard chin-to-chest contacts, indicating that chin-to-chest contact severity is mitigated in the LODC design. LODC abdomen pressures and belt penetrations discriminated between restraint conditions. These results suggest the LODC has biofidelic characteristics that make it a candidate for improved assessment of injury risk in restraint system development.

KEYWORDS – LODC, Hybrid III 10 Year Old, Biofidelity, Anthropomorphic Test Device, BioRank

INTRODUCTION

Children aged 6 – 12 represent a unique motor vehicle occupant population, as they are in the transitional phase from belt-positioning booster seats to vehicle restraints. Occupants in this age group are vulnerable to head contact with interior vehicle structures if they are not appropriately restrained for their age and size (Durbin et al. 2005, NHTSA 2005, Bidez et al. 2007). Head injuries continue to be the leading cause of pediatric fatality in motor vehicle crashes (NHTSA 2010). This occupant group is also susceptible to lap belt-induced abdominal injuries if they are not yet tall enough for the vehicle restraint (Arbogast et al. 2005, Kent et al. 2006).

To evaluate how effectively restraint systems protect against contact-induced head injuries, lap belt-induced abdomen injuries, and other injuries that frequently occur in poorly restrained child occupants, child-sized anthropomorphic test devices (ATDs) with responses and anthropometry scaled from adult data are used (Irwin and Mertz, 1997, Mertz et al. 2001, Lemmen et al. 2013). However, ATDs that represent children in the 6 - 12 year old age range have been demonstrated to exhibit differing kinematic characteristics than children (Sherwood et al. 2002, Arbogast et al. 2009, Ash et al. 2009, Lopez-Valdes et al. 2010, Seacrist et al. 2010, Wu et

Address correspondence to Dr. Jason Stammen, 10820 State Route 347, East Liberty OH 43319. Electronic mail: jason.stammen@dot.gov

al. 2013). These kinematic discrepancies, along with the lack of an injury predictive abdomen, have been problematic for evaluating large belt-positioning booster seats in Federal Motor Vehicle Safety Standard (FMVSS) No. 213 (NHTSA 2012a). These human-ATD comparison studies have all pointed toward the rigid thoracic spine as a primary factor causing extreme head rotational velocities and elevated estimation of head and neck injury, even in cases where a child is seated appropriately and unlikely to be seriously injured (Stammen et al. 2012a, NHTSA 2012a). This kinematic behavior can lead to hard chin-to-chest contacts that cause head acceleration spikes and high neck loads, which ultimately led to omission of any head or neck injury criteria for the Hybrid III 10 year old (HIII-10C) in FMVSS No. 213 (NHTSA 2012a).

Motor vehicle crash injury data indicates that if a child is seated in an age/size appropriate restraint, serious head injuries are rare (NHTSA 2010). However, without a child ATD that exhibits biofidelic response characteristics, it is challenging for restraint designers to improve their systems to mitigate non-standard head injury causation scenarios, such as offset crashes causing impact to the door or B-pillar (Bohman et al. 2011a) and torso rollout due to pre-crash avoidance maneuvers or naturalistic riding conditions (Bohman et al. 2011b, Forman et al. 2011, van Rooij et al. 2005, Andersson et al. 2010, Jakobsson et al. 2011).

In addition to the need for producing more realistic head and spine kinematics to protect children from these head injury causation scenarios, another important requirement for a child ATD representing a child occupant transitioning from child restraint to vehicle restraint is to measure the risk of abdomen injury. This measurement capability would help to assure that a child occupant will not submarine under the lap belt, which is most likely to occur when a child is not yet tall enough for the vehicle restraint to fit properly (Arbogast et al. 2005). Currently, the HIII-10C does not have measurement capability for abdominal loading. There are three main challenges in developing a biofidelic, instrumented abdomen for a child ATD: (1) biofidelic abdomen stiffness, (2) realistic pelvis anthropometry, and (3) instrumentation. A development effort to address all three challenges has already been undertaken in developing a modified abdomen/pelvis retrofit package for the Hybrid III 6 year old (HIII-6C) ATD (Arbogast et al. 2005, Kent et al. 2006, Reed et al. 2009, Klinich et al. 2010). The stiffness response of the abdomen and anthropometry of the pelvis have been completed in that effort, but the instrumentation scheme to monitor belt penetration in the fluid-filled abdomen is still under development.

While the HIII-10C has been targeted as a child ATD in need of improved biofidelity, the practical advantage of the Hybrid III design platform is that the rigid thoracic spine "box" provides a stable location for rib connection as well as for housing instrumentation. Introducing flexibility into the thoracic spine creates challenges for rib attachment and instrumentation mounting because of the mobile reference frame. Flexibility in the spine also creates a new boundary condition for the abdomen as well as packaging challenges for protection of spine, abdomen, and chest instrumentation. In addition, improvements in biofidelity could potentially degrade durability and repeatability of the ATD given the need for softer materials and more moving parts. Therefore, achievement of biofidelity requires not only the thoracic spine to be made more flexible but also that it be integrated with the neck, shoulders, ribcage, abdomen, and pelvis in a manner that ensures durability, repeatability, and protection of instrumentation housed within the ATD.

NHTSA initiated a project in 2011 that leverages recently generated pediatric information to guide the development of a new ATD - the **L**arge **O**mni**D**irectional **C**hild (LODC). The LODC is similar in size to the HIII-10C and has a flexible thoracic spine, instrumented abdomen, and improved anthropometry. The purpose of this paper is to introduce the LODC ATD design features and compare its body region responses and full body performance characteristics with both HIII-10C ATD responses and pediatric biomechanical requirements. While improved biofidelity is a primary consideration for evaluating LODC performance in this paper, aspects such as durability and repeatability are also priorities for the usability of the ATD and are addressed as well herein.

LODC DESIGN OVERVIEW

The LODC has several features that distinguish it from the Hybrid III 10 year old ATD, including a head with pediatric inertial properties, a flexible thoracic spine, a two-piece ribcage assembly, shoulders with anatomic mobility, a neck that permits elongation and atlanto-occipital joint rotation, a biofidelic abdomen with both pressure and belt penetration measurement capability, and a pelvis reflecting seated child anthropometry (Figure 1). Each body region has been addressed with the exception of the lower arms and thighs/legs (both of which are the same as the HIII-10C).

Anthropometry. The LODC ATD is designed to represent a 9 – 11 year old child, with a stature matching the HIII-10C but detailed anthropometry matching 10 year old seated volunteer model data from Reed et al. (2006, 2009) (Figure 2, Tables 1-2).

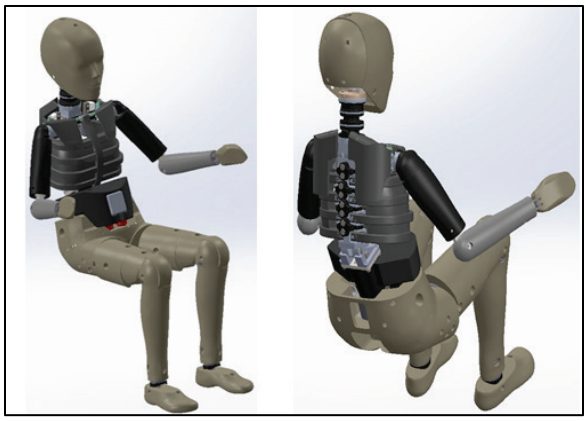

Figure 1. Large Omnidirectional Child (LODC) ATD (with torso flesh & jacket removed)

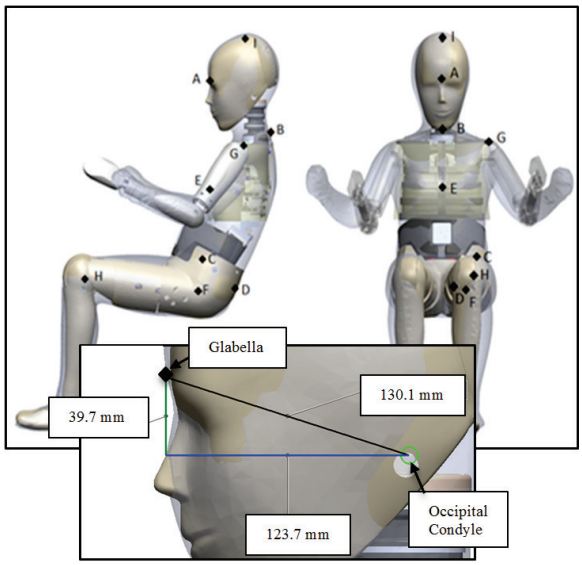

Figure 2. Overlay of LODC with UMTRI Childshape model (www.childshape.org)

Table 1. Childshape* landmark coordinates associated with LODC anthropometry (values shown are in millimeters and relative to the hip joint location)

Human Landmark	Figure 2 ID	X	Y	Z
Glabella	A	28.9	67.5	506.6
Occipital condyle (with respect to Glabella)	see inset	123.7	---	-39.7
C7 posterior spine	B	189.2	67.7	384.6
Anterior superior iliac spine	C	9.6	-26.7	78.3
Posterior superior iliac spine	D	99.6	32.5	8.9
Substernale	E	28.0	64.9	245.1
Hip joint	F	0.00	0.00	0.00
Acromion	G	118.4	-60.3	355.3
Knee joint center	H	-302.5	161.9	31.6
Top of head	I	136.7	61.5	586.4

*Childshape inputs were stature = 1300, BMI = 20, SHS = 55, recline = 20, flex = 45

Table 2. Comparison of external dimensions and segment masses

Parameter	LODC	HIII-10C	Childshape model	9-11YO Volunteer Data from Reed et al (2006)	9-11YO CDC Growth Charts (50th Percentile, 2000)***
Mass, overall (kg)	34.6	35.2	---	36.1 ± 5.7	28.5 – 37.0
Mass, head (kg)	3.56	3.73	---	---	---
Mass, neck (kg)	0.53	0.80	---	---	---
Mass, upper torso (kg)	6.62	8.15	---	---	---
Mass, lower torso (kg)	10.12	8.72	---	---	---
Body mass index (kg/m^2)	20	20	20	18.1 ± 2.4	16.2 – 17.5
Stature (mm)*	1300	1300	1300	1413 ± 58.6	1330 - 1440
Seated height (mm)**	679	716	684	692 ± 5.7	---
Erect Sitting Height / Stature	0.55	0.586	0.55	0.52 ± 0.01	---
Shoulder width (mm)	340	315	343	---	---
Shoulder height (mm)	390	395	394	---	---
Chest depth (mm)	188	165	185	---	---
Chest circumference (mm)	755	704	720	---	---
Abdomen depth (mm)	182	186	196	---	---

*LODC stature was designed to be the same as the HIII-10C stature; both dummies have short legs in comparison to volunteers but matching seated height; **Calculated as Seated Height = Erect Sitting Height * COS(20 deg), where 20 degrees is the recline angle; ***Range is combined boys and girls 50th percentile values from age 9 - 11

Head. The LODC head is a HIII-10C head, but with modifications to match the inertial properties of a similar age (9 year old) pediatric specimen (Loyd et al. 2010). Specifically, the mass is reduced and center of mass moved upward and forward to match the pediatric data, primarily by adding a tungsten ballast plug to the top of the skull, removing mass from the skull cap, and removing material from the mandible area. In addition, a forehead head skin insert was implemented to tune the impact response. Figure 3 describes how the skull, skull cap, and head skin were modified, and Table 3 compares the head mass properties with human head characteristics.

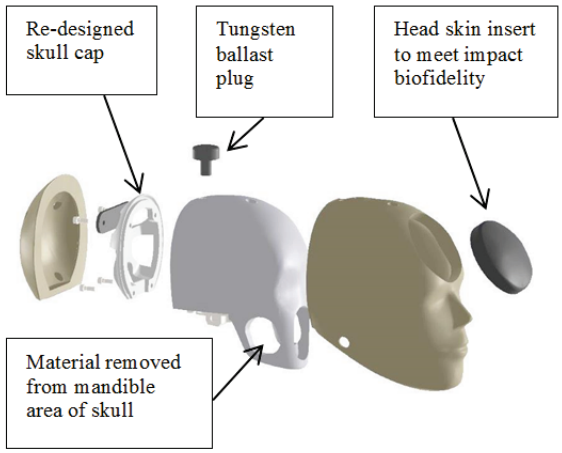

Figure 3. LODC head design

Table 1. LODC head mass properties

Parameter	10YO Human [from Loyd 2009]	LODC	HIII-10C
Mass (kg)	3.56	3.56	3.73
X Distance from Head CG to OC (mm)	19.2*	18.0	11.5
Z Distance from Head CG to OC (mm)	52.8	53.4	43.2
Moment of Inertia about X, I_{xx} (mm^4)	0.0135	0.0106	0.0099
Moment of Inertia about Y, I_{yy} (mm^4)	0.0164	0.0148	0.0153
Moment of Inertia about Z, I_{zz} (mm^4)	0.0119	0.0142	0.0145

*Reported value for a 9 year old specimen. No correlation was found for head CG to OC X distance with respect to characteristic length for the development of a predictive model. Adult specimens averaged 23 mm, while a 6 year old specimen was 8.5 mm.

Neck. The LODC neck has several features that set it apart from other ATDs. First, the neck has a low profile mechanism between the modified occipital condyle plate and top plate of the neck that consists of internal and external mating plates, a Teflon ring, and rubber twist stops. This mechanism provides ±20 degrees of free rotation about the Z axis just below the occipital condyle (Figure 4). This feature was implemented because it was observed in human neck specimens that very little resistance is present in pure neck torsion loading at angles below 40 degrees (Myers et al. 1989). In the LODC neck, there is no resistance until the stops are reached.

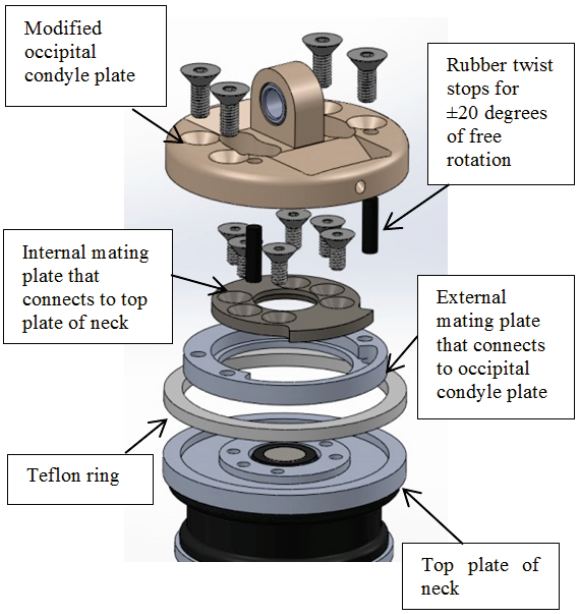

Figure 4. LODC neck twist mechanism

The neck is made from damped chlorobutyl rubber (Shore A 80 durometer) to achieve the appropriate dynamic phase lag in flexion loading. The vertebral segments have different shapes that have been tuned to deliver the necessary translational head lag observed in human frontal response (Thunnissen et al. 1995). Soft nodding blocks are incorporated as well to tune angular head lag with respect to the neck. The internal cable permits up to 10 mm of neck elongation and is over molded with transparent silicon rubber to limit cable wear and interference with surrounding metal components (Figure 5). The LODC neck cable position is fixed at the inferior end of the neck assembly, so there is no requirement to set and maintain the cable torque within a specified range, as is the case with the HIII-10C.

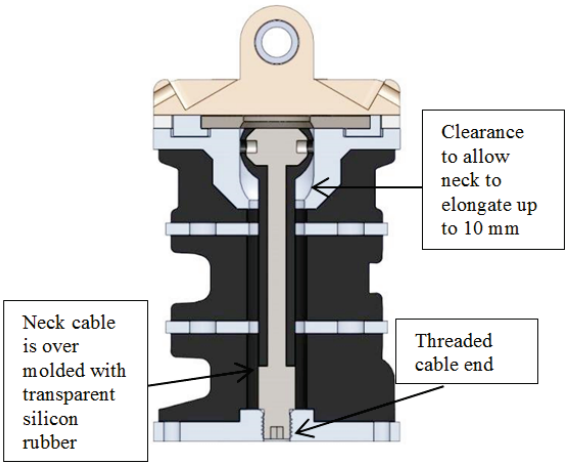

Figure 5. LODC neck design

Thoracic Spine. The LODC thoracic spine contains four soft vertebral elements that are stabilized through dual laminated linkage assemblies on the posterior aspect of the spine, with anterior connecting links to stabilize the joints (Figure 6). Each vertebral level has a location for both an InfraRed - Telescoping Rod for Assessment of Chest Compression (IR-TRACC) and a 3aω motion package that includes three accelerometers and three angular rate sensors to calculate six degree of freedom motion. The lumbar spine connects the inferior surface of the thoracic spine to the pelvis at an angle reflecting child anthropometry (Reed et al. 2009). The cervicothoracic and thoracolumbar spine junctions both have angle adjustability. To provide repeatable positioning given the increased mobility, a removable tool is used to maintain the spine in a standardized posture during seating. The tool is routed through a series of ABS routing elements on the lateral aspect of each spine element. Implementation of this tool required a small access hole to be added to the jacket, and it is designed to be easy to remove once the ATD is seated.

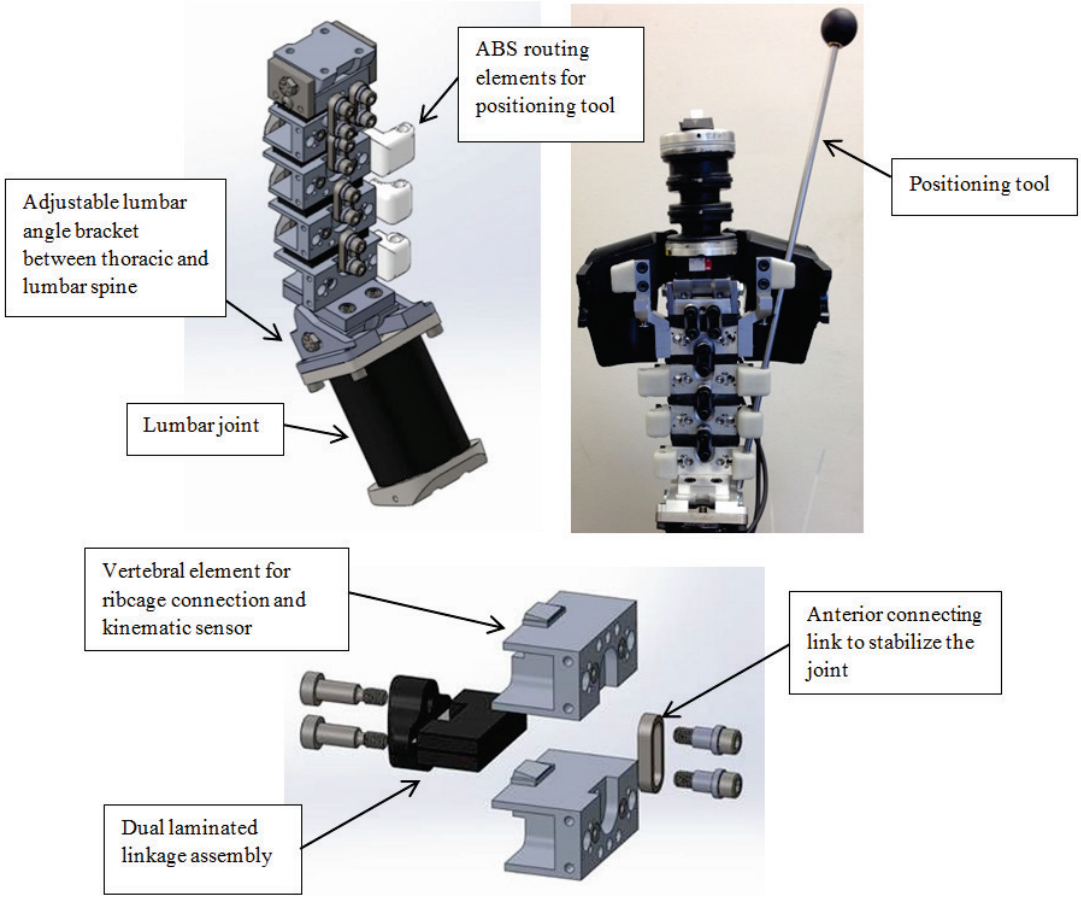

Figure 6. LODC spine design

Thorax. Current Hybrid III child frontal ATDs have ribcage structures with the same general construction as adult frontal ATDs. The LODC ribcage has an entirely different structure that consists of an over molded cable construction that provides stability in the connections to the spine and sternum. The ribcage is a two-piece, hemispherical structure with a smooth, continuous internal surface that protects internal instrumentation and cabling from sharp edges as well as preventing relative rib motion (Figure 7). The assembly allows for up to four IR-TRACCs, which can be oriented in either lateral or frontal directions. Externally, the LODC has a ½" thick soft silicon rubber wrap that encompasses the ribcage to simulate human soft tissue. A neoprene suit covers the upper and lower torsos.

The shoulder includes a clavicle and pronounced scapula to provide a surface for the shoulder belt, a ball and socket configuration at the glenohumeral joint, and an upper ribcage stiffener at the ATD mid-sagittal plane to prevent the clavicles from collapsing into the spine (Figure 8). The scapulae connect to the thoracic spine by way of a pivot that permits rotation about the Z axis while maintaining resistance in the X direction.

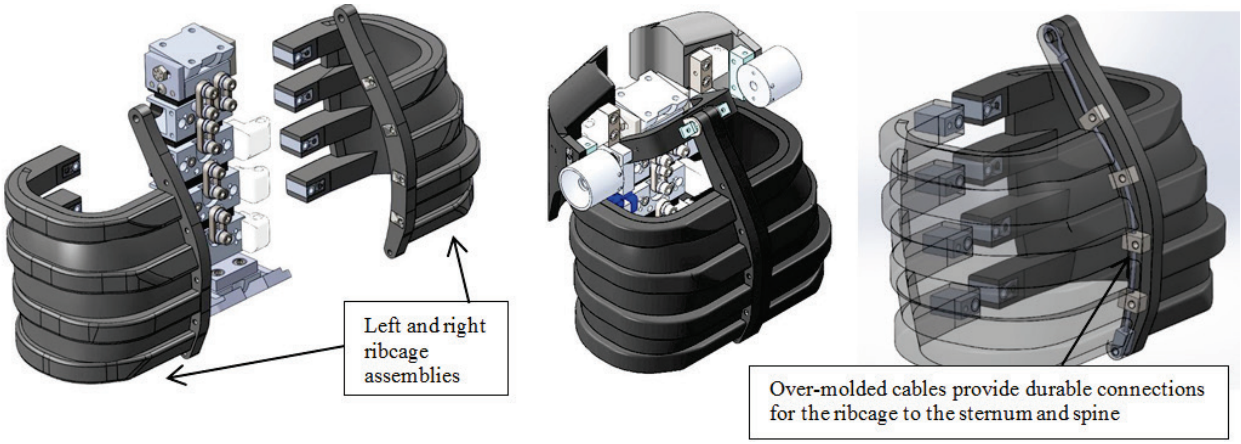

Figure 7. LODC thorax design

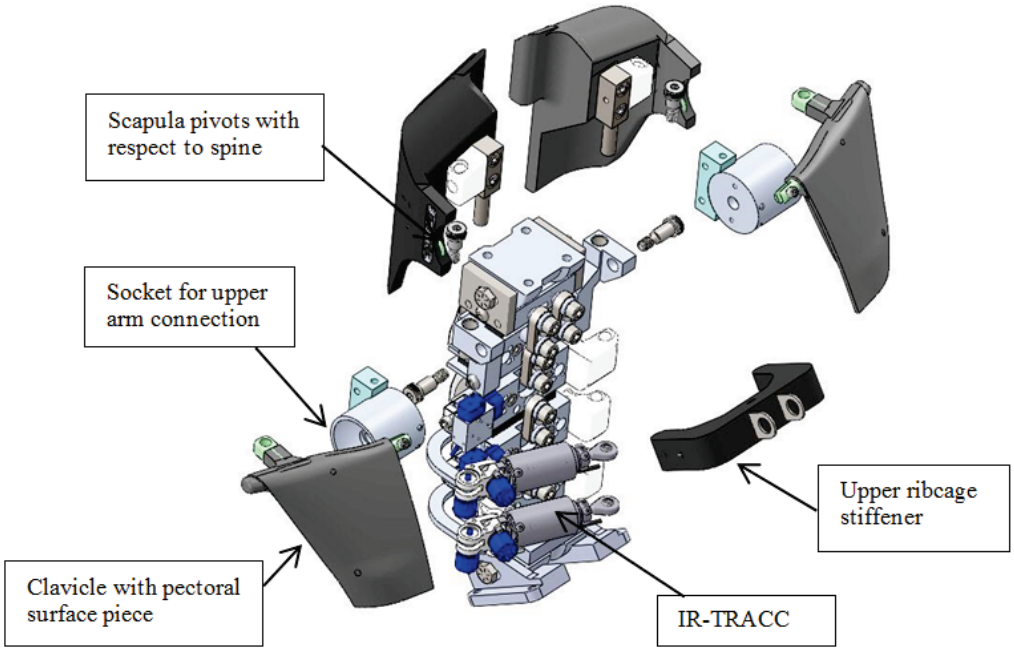

Figure 8. LODC shoulder design

Abdomen & Pelvis. The LODC abdomen contains left and right pressure sensors (Abdominal Pressure Twin Sensors (APTS), Transpolis) and a 3aω block motion pack. The 3aω block is attached to the rear side of an aluminum cup that seats into a corresponding recess in the abdomen so that the cover plate of the cup is flush with the abdomen surface (Figure 9). The 3aω sensor wires route vertically down the front of the abdomen then rearward under the abdomen and out the back of the pelvis assembly. Abdominal penetration is calculated by first integrating 3aω motion at the abdomen surface, pelvis, and T12 (top of lumbar) locations, transforming to the global X axis, then subtracting the average pelvis/lumbar displacement from the displacement of the front abdomen surface. The relative construction and geometry of the abdomen and pelvis in the Hybrid III child ATDs have been shown to differ from human anthropometry (Reed et al. 2009). The LODC pelvis was therefore modified similarly to the Hybrid III 6C as described by Klinich et al. (2010), with removal of the anterior pelvis vinyl skin from the HIII-10C pelvis so that the abdomen extends past the front of the ASIS bones.

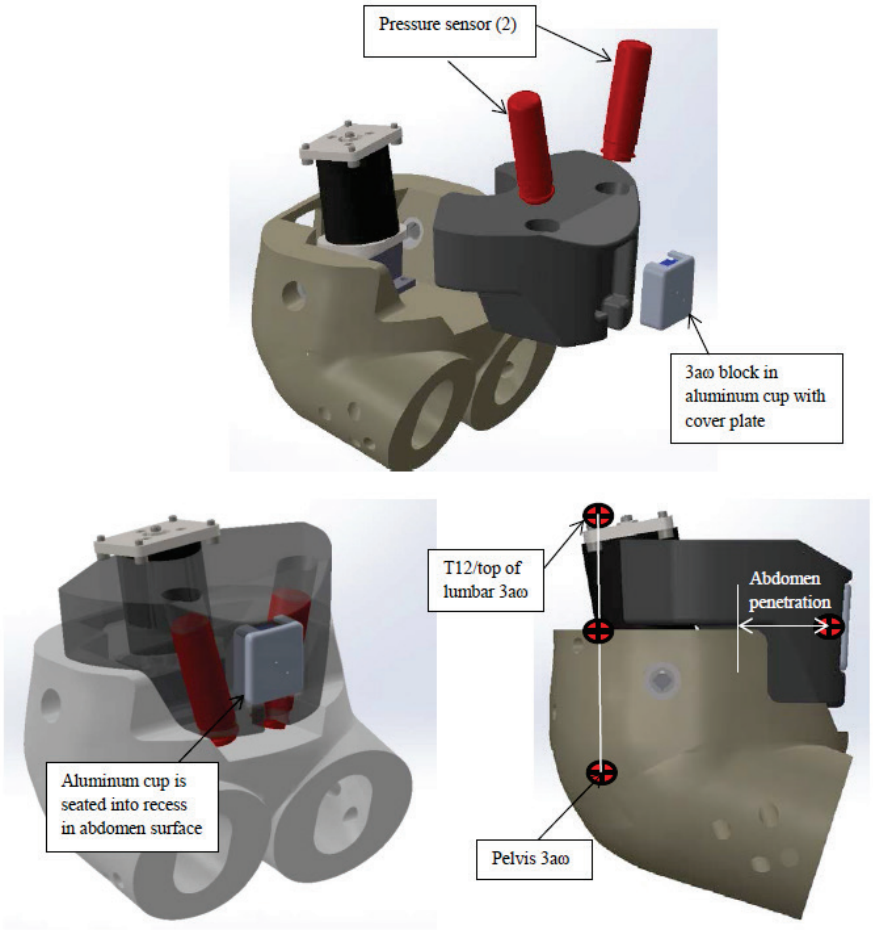

Figure 9. LODC abdomen & pelvis design

BODY REGION BIOFIDELITY

The first objective of this study was to evaluate the LODC body region responses against biomechanical data. Tests were conducted on the head, neck, cervicothoracic spine, thorax, and abdomen. Biomechanical tests were selected for the evaluation of each LODC body region based on the relevance to ATD design in terms of impact response (the test should simulate how the ATD will be loaded by the system it is evaluating), anthropometry (the data collected should be from pediatric specimens similar in size to LODC), inertial properties (the mass and moment of inertia of the body segment reflect human

mass distribution), and kinematics in conditions similar to how the LODC will be used to evaluate restraints (i.e. full body tests simulating a crash such as FMVSS No. 213). From a practical standpoint, the selected tests need to be repeatable and the test fixtures should be easily accessible or defined fully so that they can be fabricated. Table 4 summarizes the selected sources of pediatric biomechanical data for this evaluation based on these criteria. It is important to note that the test conditions selected for this study are not meant to be exclusive for the development of the LODC. Other test conditions not included in this component biofidelity evaluation will surely be considered as the LODC evolves and new biomechanical studies are presented in the future.

Table 4. Pediatric biomechanical tests selected for ATD body region evaluation

Body Region	Test Specifications	Source(s)
Head	CFR Part 572 Subpart T HIII-10C test procedure, except that drop heights were limited to 150 and 300 mm	Loyd et al. (2009, 2016)
Neck	CFR Part 572 Subpart T HIII-10C neck flexion test procedure at 6.1 m/s	Dibb et al. (2014)
Cervico-thoracic Spine	Mini-sled frontal flexion test with head-neck-upper thoracic spine segment at 4.0 m/s	Kang et al. (2016)
Thorax	CFR Part 572 Subpart T, 6.89 kg probe impact test at 6.0 m/s	Parent et al. (2010)
Abdomen	Fixed back belt pull test at 3.0 m/s	Kent et al. (2006)

Biomechanical Requirements & Dynamic Test Setups

Both the LODC and HIII-10C were evaluated in the test conditions listed in Table 4. While the LODC is intended to be "omnidirectional" with frontal, lateral, and oblique response characteristics, the HIII-10C was only designed for frontal loading. Therefore, the LODC and HIII-10C were only compared in frontal conditions. These frontal test conditions are described in detail next.

Head. Loyd et al. (2009, 2016) generated age-dependent head impact response biofidelity targets from pediatric PMHS specimens (Figure 10). The acceleration vs. time pulse in the PMHS head drop was estimated by dividing the force plate time history by the drop mass, with HIC calculated from that pulse. Standard deviation percentages from repeated adult head tests were applied to the 9YO pediatric data, as an estimate of variation if the pediatric head was actually tested multiple times.

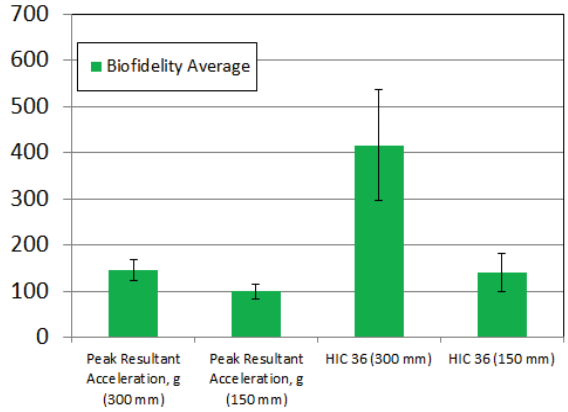

Figure 10. Head impact biofidelity targets from Loyd et al. (2009, 2016)

LODC and HIII-10C head impact tests were conducted at 150 mm and 300 mm drop heights to match the pediatric specimen test drop heights. The Code of Federal Regulations (CFR) 49 Part 572 test procedure (NHTSA 2012b) was used for positioning, releasing, and aligning the ATD head so that impacts to the drop plate were located at the forehead portion of the head (Figure 11). Three tests were conducted at both drop heights with a 30 minute recovery period between tests, so that repeatability could also be evaluated.

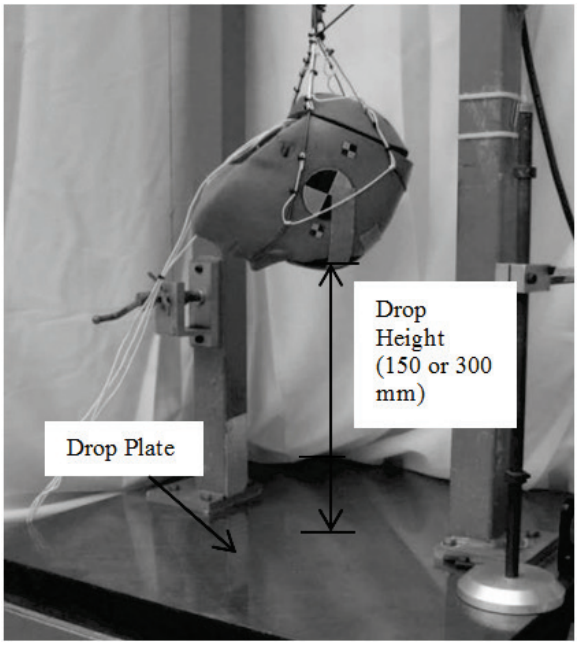

Figure 11. Head drop test setup

Neck. Dibb et al. (2014) generated neck moment vs. rotation response requirements for a 10 year old ATD by simulating a CFR Part 572 Subpart T test (6.1 m/s) with a pediatric head-neck model developed from pediatric biomechanical data obtained through head (Loyd et al. 2009) and neck (Luck et al. 2008) tests conducted on pediatric specimens (Figure 12). This corridor was created by performing an uncertainty analysis with various muscle activation settings in the neck portion of the model. LODC and HIII-10C neck flexion tests were conducted according to the same CFR 49 Part 572 test procedure (Figure 13). To assess repeatability, three repeat tests were conducted.

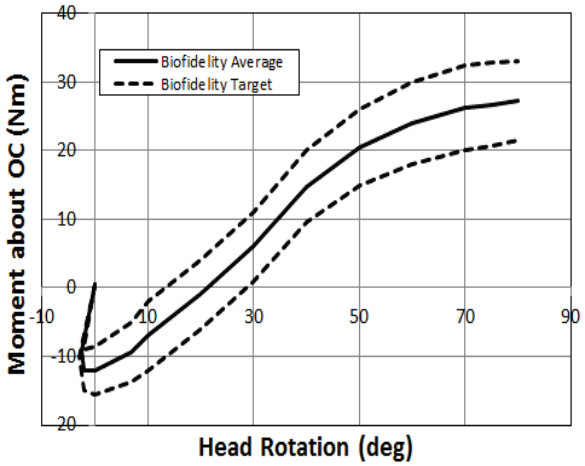

Figure 12. Neck flexion biofidelity target from Dibb et al. (2014)

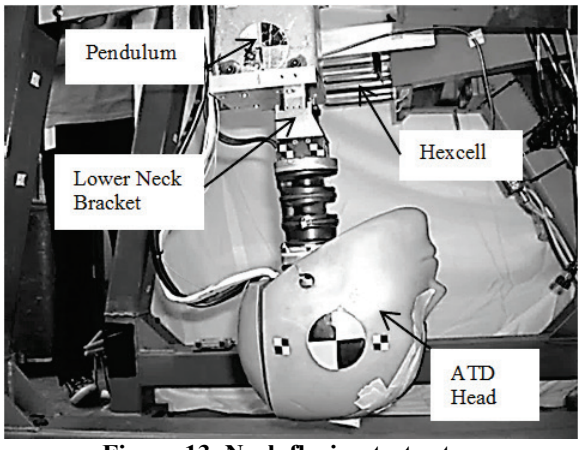

Figure 13. Neck flexion test setup

Thoracic Spine. In Kang et al. (2016), an adult PMHS body section comprised of the head, neck, and upper thoracic spine structures was tested at nominal 4.0 m/s in the frontal loading condition as shown in Figure 14 (see Appendix A for more details on the PMHS setup). The mini-sled pulse was developed to match the first thoracic spine vertebra (T1) acceleration of a three-point belt restrained LODC subjected to a FMVSS No. 213 sled test. Upper and lower neck loads, as well as head kinematics from three PMHS were measured in these tests.

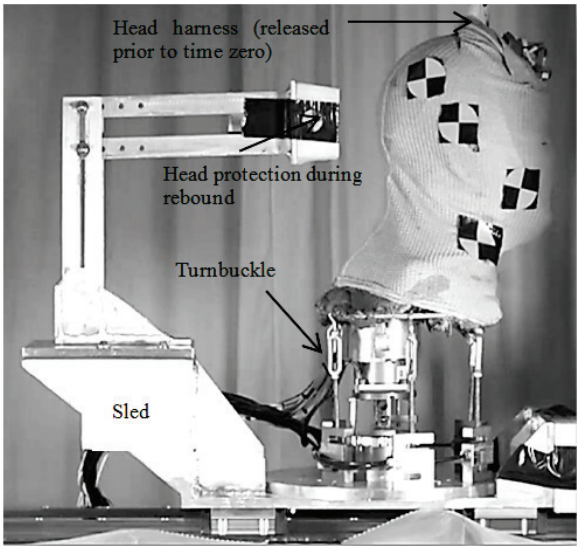

Figure 14. PMHS setup from Kang et al. (2016)

The data was scaled to a 10 year old size using mass scaling (Eppinger et al. 1984, Mertz et al. 2001) based on head & neck combined mass rather than whole body mass, given only this segment of the body was tested. Biofidelity targets where then created for the individual channel time channels using the methodology from Kang et al. (2012). Figures 15-16 show the resulting biofidelity targets.

The test condition used to evaluate the LODC and HIII-10C head, neck, and top thoracic spine assembly is shown in Figure 17. Both ATDs were tested under the same loading conditions as the PMHS, except that the LODC ATD head was supported by pre-cut masking tape rather than the full head harness prior to the test (Figure 17). High speed video analysis (TEMA software, Image Systems Motion Analysis) was used to evaluate neck kinematics to compare with neck data from the adult PMHS in Kang et al (2016). A load cell was connected to the mini-sled and the T3 spine element bracket was coupled to the load cell by way of an adaptor plate. Three repeat tests were done with the LODC to assess repeatability.

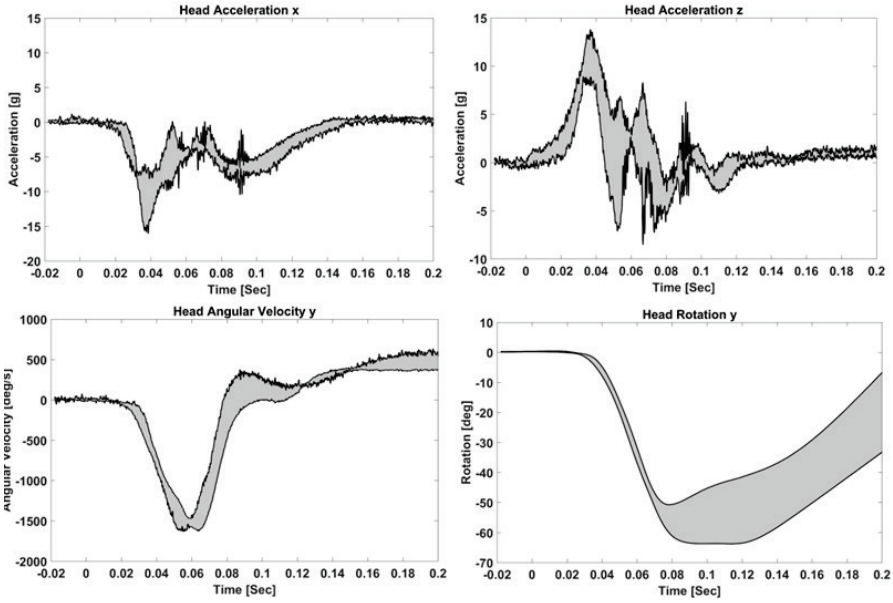

Figure 15. Head kinematic biofidelity targets developed from Kang et al. (2016)

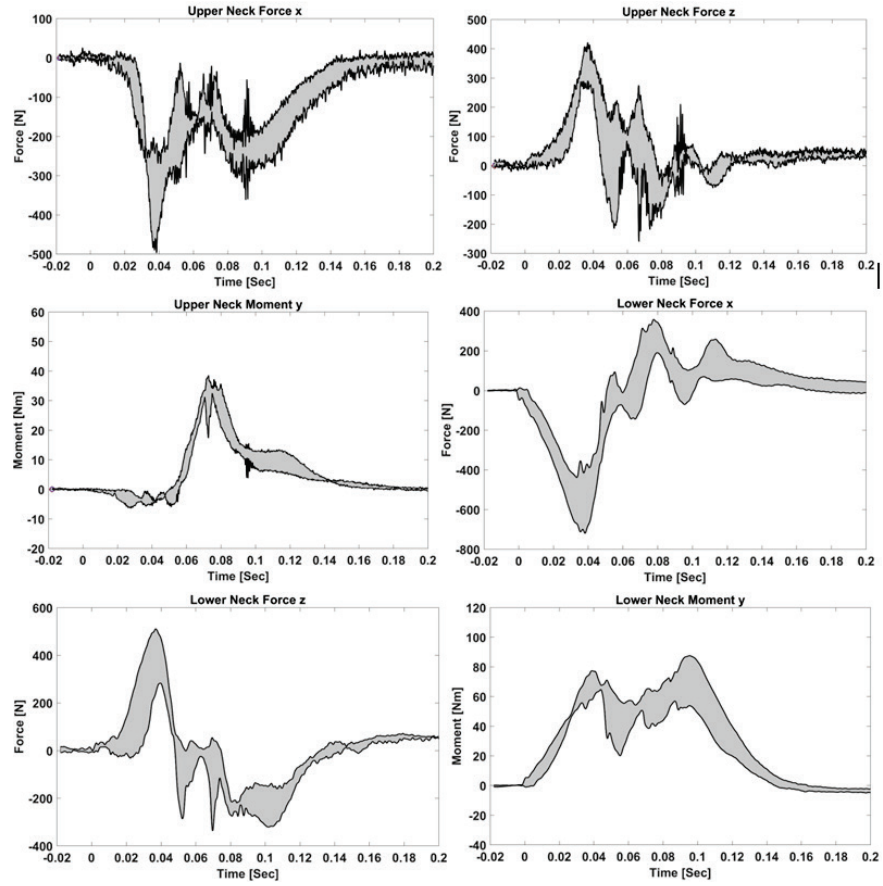

Figure 16. Upper and lower neck load biofidelity targets from Kang et al. (2016)

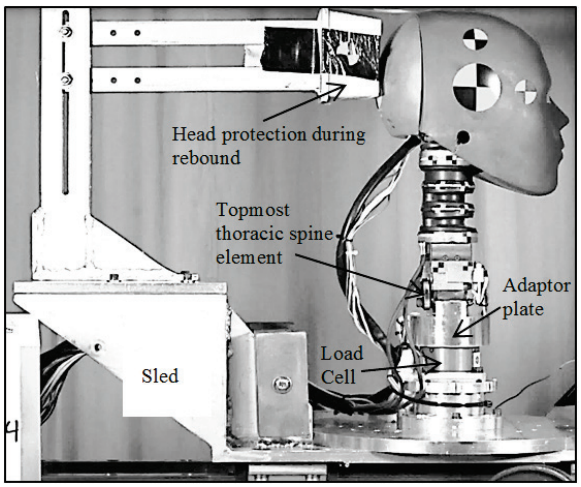

Figure 17. LODC dynamic mini-sled test setup replicating PMHS setup shown in Figure 14

Thorax. Parent et al. (2009, 2010) re-processed pediatric PMHS test data from Ouyang et al. (2006) and developed scaled impact response corridors applicable to the blunt impact response of a 6 year old ATD. This re-processed data was then extended to a 10 year old size ATD by scaling both the mass and velocity of the impact probe according to Irwin et al. (2002). Figure 18 shows the resulting biofidelity target for the thorax response of a 10 year old size ATD.

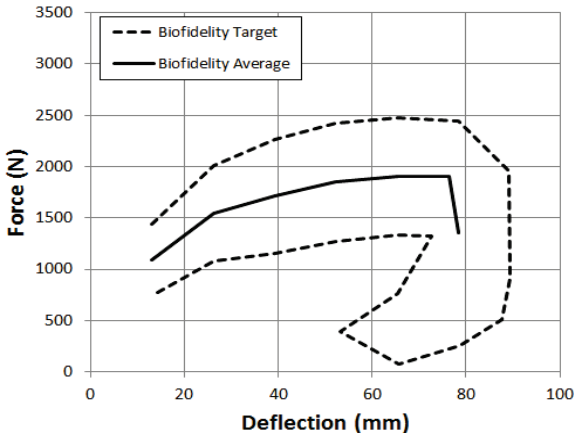

Figure 18. Thorax biofidelity target for a 10 year old sized ATD (external deflection shown)

The LODC and HIII-10C were tested using CFR 49 Part 572 conditions for the HIII-10C (Figure 19). Tests were conducted at 6.0 m/s with the Part 572 size impact probe (6.89 kg, 152 mm diameter face). Force was calculated by multiplying the probe mass by the probe acceleration, and the deflection was calculated by subtracting the chest acceleration from the probe acceleration and double integrating the signal. Deflection was calculated in this manner for both ATDs instead of using internal chest deflection (IR-TRACC or potentiometer) because the biofidelity corridor was derived using externally measured deflection. The center of the impactor was centered on the second rib in line with the IR-TRACC mounted at the rib 2 location within the dummy. The LODC thorax and head are set vertical so that the probe face contacts the thorax surface uniformly. This alignment assured minimal off-axis loading of the IR-TRACC and clearance between the lower edge of the probe and top of the abdomen.

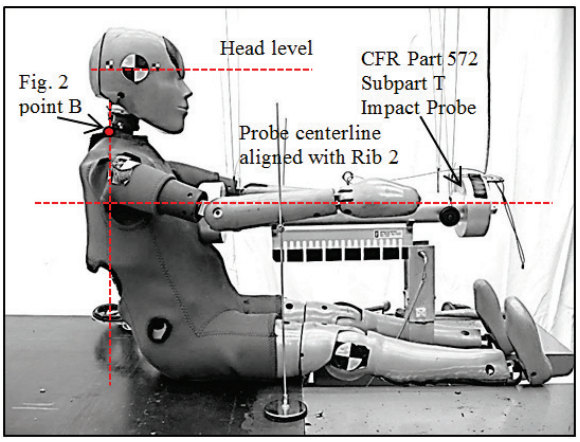

Figure 19. LODC thorax impact setup

Abdomen. Kent et al. (2006) tested a series of porcine specimens that were developmentally matched to human pediatric ages, and later these responses were verified for evaluating child ATDs by demonstrating that pediatric PMHS response were consistent with the porcine data in the same test condition (Kent et al. 2011). The biofidelity envelope created from this testing is shown in Figure 20.

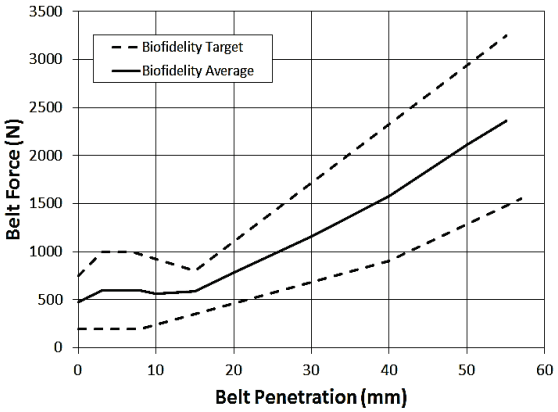

Figure 20. Lower abdomen biofidelity target derived from Kent et al. (2006) data

The LODC and HIII-10C abdomen dynamic responses were evaluated by employing a similar (but not identical) fixed back setup (Figure 21) as used previously to test porcine specimens and later for pediatric PMHS (Kent et al. 2011). The ATD is seated upright instead of supine, similar to the setup employed previously to test adult PMHS abdomens (Foster et al. 2006, Lamielle et al. 2008). A reinforced seatback frame was fixed in place, so that the ATD's back was supported. A two inch width vehicle belt was connected to a T-bar that was pulled rearward at a nominal velocity of 3.5 m/s by a hydraulic ram. A string potentiometer was connected to the midline of the belt in the ATD mid-sagittal plane at approximately the level of the umbilicus to measure belt penetration. Because of the difference in pelvis structure between the LODC and HIII-10C, the belt was positioned at the same height from the table for both ATDs. This step resulted in the belt mid-line being coincident with the pelvis rim on the HIII-10C. Belt tension load cells on the left and right sides of the ATD measured the belt force. The LODC abdomen was equipped with abdomen pressure sensors (filtered at CFC1000) to measure pressure due to belt loading.

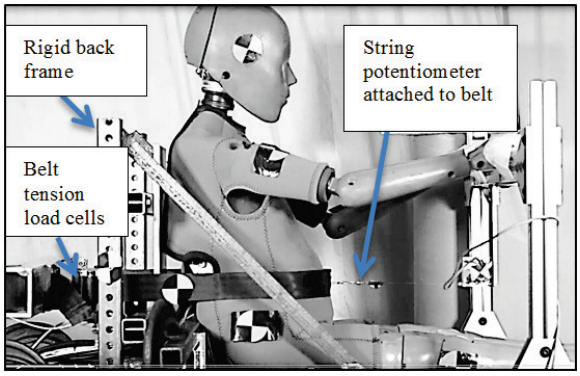

Figure 21. LODC abdomen belt pull setup

Biofidelity Analysis Methodology

The relative biofidelity of the LODC and HIII-10C was quantified using the Biofidelity Ranking System ("BioRank") methodology. The BioRank calculation assesses the biofidelity of an ATD by comparing the dummy response to the mean cadaver response, as originally defined by Rhule et al. (2002) and later updated to minimize subjective weighting of test conditions in Rhule et al. (2009). To account for the variability in individual cadaver responses, BioRank calculates a cumulative variance between the dummy response and the mean cadaver response (DCV) and normalizes this value by the cumulative variance between the mean cadaver response and the mean plus one standard deviation cadaver response (CCV).

$$\text{BioRank Score} = \sqrt{R} = \sqrt{\frac{DCV}{CCV}} = \sqrt{\frac{\sum (Y(x_i)_{ATD} - Y(x_i)_{human})^2}{\sum (\sigma(x_i)_{human})^2}}$$

The standard deviation, σ, represents the variance in the responses of a finite number of subjects:

$$\sigma = \sqrt{\frac{1}{N}\sum_{i=1}^{N}(x_i - \mu)^2}$$

For time histories, the time scale over which the BioRank score is calculated is dictated by the peak value of the mean cadaver response. Only dummy data occurring within the time range in which the cadaver mean value is within 80% of the peak cadaver value is included in the analysis (i.e., excludes low magnitude tails). A BioRank value of 0.0 would indicate an ATD response identical to the biofidelity corridor mean; a value of 1.0 would indicate an ATD response that is on average one standard deviation away from the corridor mean; and a value of 2.0 would indicate an ATD that is considered to respond as much like the corridor as another PMHS.

In order to obtain PMHS response corridors appropriate for the calculation of DCV and CCV, three different approaches were considered. A decision was made in each test condition based on the available information.

1. Acquisition of a response corridor presented in the literature. As long as the corridor width is clearly defined in terms of standard deviation, the corridor can be used as stated.
2. Acquisition of the individual responses presented in the literature. This approach requires re-calculation of the response corridor.
3. For conditions that did not allow for either of the above approaches, BioRank was calculated using single point measures such as the peak force or peak deflection.

The approach taken in each test condition is described in the relevant sections. In each of the five test conditions, the ATD tests were repeated multiple times. In these cases, the mean ATD response was used in the calculation of BioRank.

For each ATD measurement, a BioRank score was calculated. Then, the BioRank scores taken from

each measurement within a body region were averaged to get a body region score. In the cervicothoracic spine condition where multiple body regions were measured, each body region score was averaged to obtain a full "test condition" score. Finally, each of the five test condition scores were averaged to get an overall ATD BioRank score.

Body Region Biofidelity: Results

Head. LODC head drop responses from three repeat tests at both 150 mm and 300 mm (Figure 22) showed excellent repeatability.

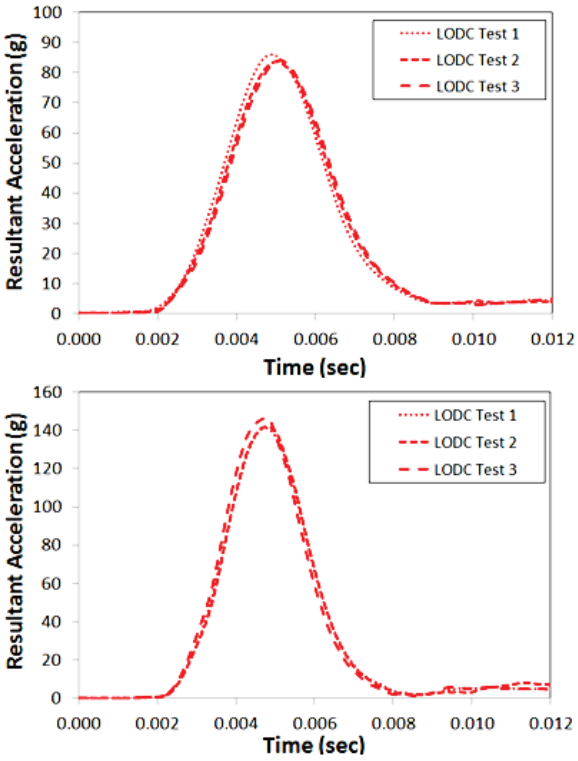

Figure 22. LODC resultant head accelerations for 150 mm (top) and 300 mm (bottom)

Because of the absence of time history data, two measures were used to characterize the overall biofidelity of the head in the BioRank calculation – HIC and peak head acceleration. Injury criterion calculations such as HIC are not typically used for BioRank scoring, but since HIC is a time integral of the resultant acceleration, it gives information on the magnitude, shape, and duration of the acceleration trace that the peak resultant acceleration does not alone provide. Figure 23 describes the ATD responses in comparison with the 9YO PMHS from Loyd et al. (2009).

Table 5 shows a significantly improved BioRank score for the LODC over the HIII-10C.

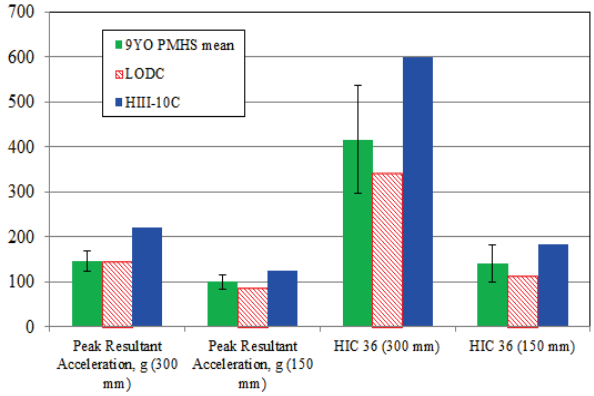

Figure 23. Head drop test biofidelity for LODC and HIII-10C vs. 9YO PMHS (Loyd et al)

Table 5. BioRank scores for LODC and HIII-10C head drop tests

Measurement	LODC	HIII-10C
Head resultant acceleration (g), 300 mm	0.12	3.21
Head resultant acceleration (g), 150 mm	0.98	1.44
HIC 36, 300 mm	0.61	1.53
HIC 36, 150 mm	0.71	1.08
AVERAGE HEAD SCORE	**0.61**	**1.81**

Neck. Figure 24 shows the excellent repeatability of the LODC neck flexion responses. Figure 25 shows the average ATD moment-rotation responses in comparison to the pediatric model based corridor. The LODC displayed similar peak moment and peak rotation to the pediatric model in the same condition. While the HIII-10C was more consistent with the corridor up until 60 degrees, sled tests typically result in neck flexion angles well above that angle. The LODC was within or near the corridor over the portion of the response beyond 60 degrees. To achieve an earlier moment increase in the 30 – 60 deg rotation window, it is suspected that the allowable elongation limit may need to be adjusted, in addition to tuning the fore/aft nodding blocks, to achieve the required response over the entire stroke. While the response does not reflect the nonlinear softening characteristics of the human model, Figure 26 indicates qualitative consistency between the LODC head-neck and pediatric head-neck model in overall kinematics.

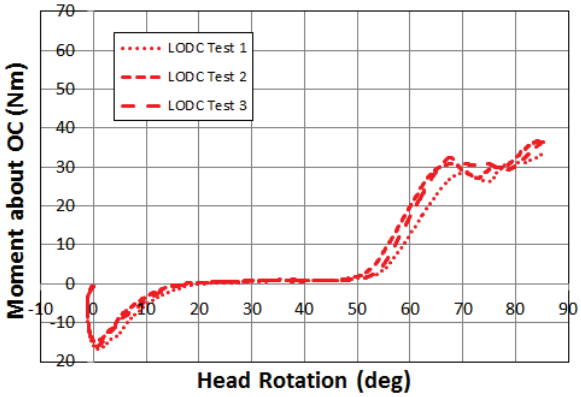

Figure 24. LODC neck flexion test repeatability

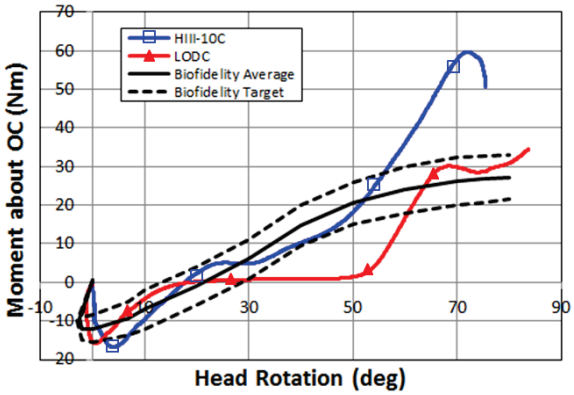

Figure 25. Neck flexion test biofidelity

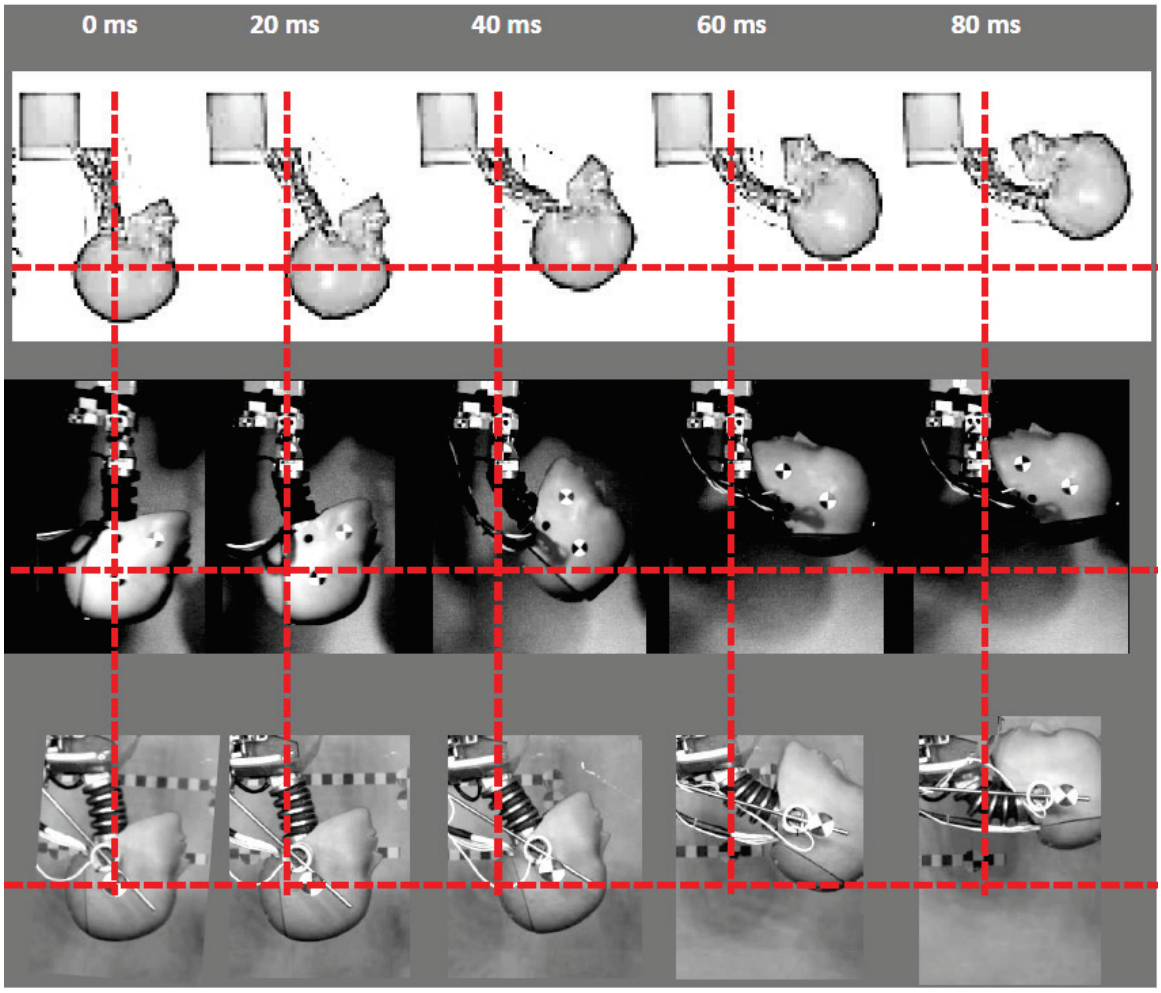

Figure 26. Pediatric model (top, Dibb et al. 2014), LODC (center), and HIII-10C (bottom)

For quantitative biofidelity assessment of the neck, moment and rotation time histories were not available. Therefore, BioRank scores were calculated by summing the difference between the respective ATD moments and the biofidelity average at each head rotation increment. The LODC response was found to be more consistent with the pediatric biofidelity target than the HIII-10C (Table 6).

Table 6. BioRank scores for LODC and HIII-10C neck flexion tests

Measurement	Formula*	LODC	HIII-10C
NECK BIOFIDELITY SCORE	$\sqrt{\frac{\sum(M(r_i)_{ATD} - M(r_i)_{human})^2}{\sum(\sigma(r_i)_{human})^2}}$	**1.57**	**2.73**

*$M(r_i)_{ATD}$ = ATD moment at a given rotation, $M(r_i)_{human}$= mean human moment at a given rotation, and $\sigma(r_i)_{human}$= human standard deviation in moment at a given rotation

Cervicothoracic Spine. Figure 27 shows the behavior of the head, neck, and topmost thoracic spine flexible element. Horizontal and vertical reference guides are provided for qualitative comparison of head center of gravity motion at each time increment. The absolute XZ planar motion of the LODC closely approximates the PMHS motion, while the HIII-10C displays much less X and Z displacement. Results for head kinematics, neck kinematics, and T3 (lower neck) loads are shown with respect to the biofidelity targets (Figures 28-31). This test condition is quite repeatable, as shown by the excellent repeatability for the three LODC tests, as the plots include all three repeat test curves. The mean response from the three repeat tests was used to calculate the BioRank score for each channel. The large positive peak in the HIII-10C head acceleration trace (0.15 – 0.18 seconds) is due to the protective foam coming loose during rebound and does not factor into the BioRank score because it is not within the time range where the mean PMHS value is within 80% of the peak PMHS (negative) value.

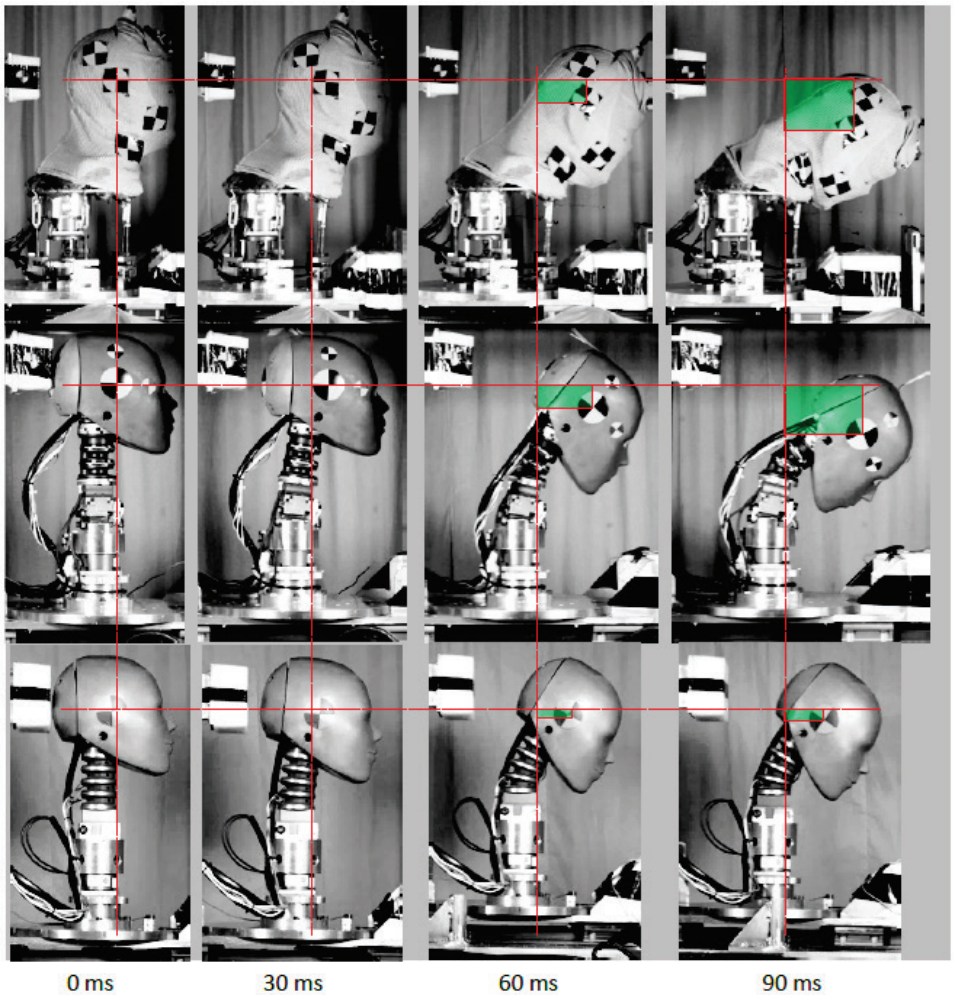

Figure 27. Adult PMHS (top, Kang et al. 2016), LODC (center), and HIII-10C (bottom)

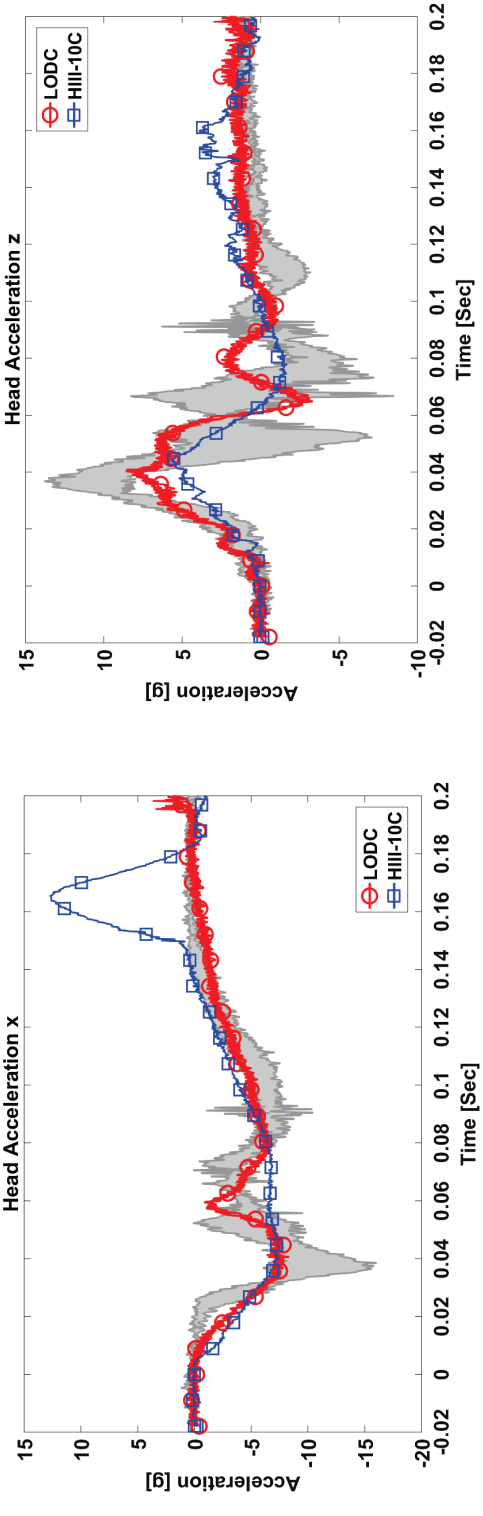

Figure 28. LODC vs. HIII-10C head accelerations (gray shaded = scaled PMHS)

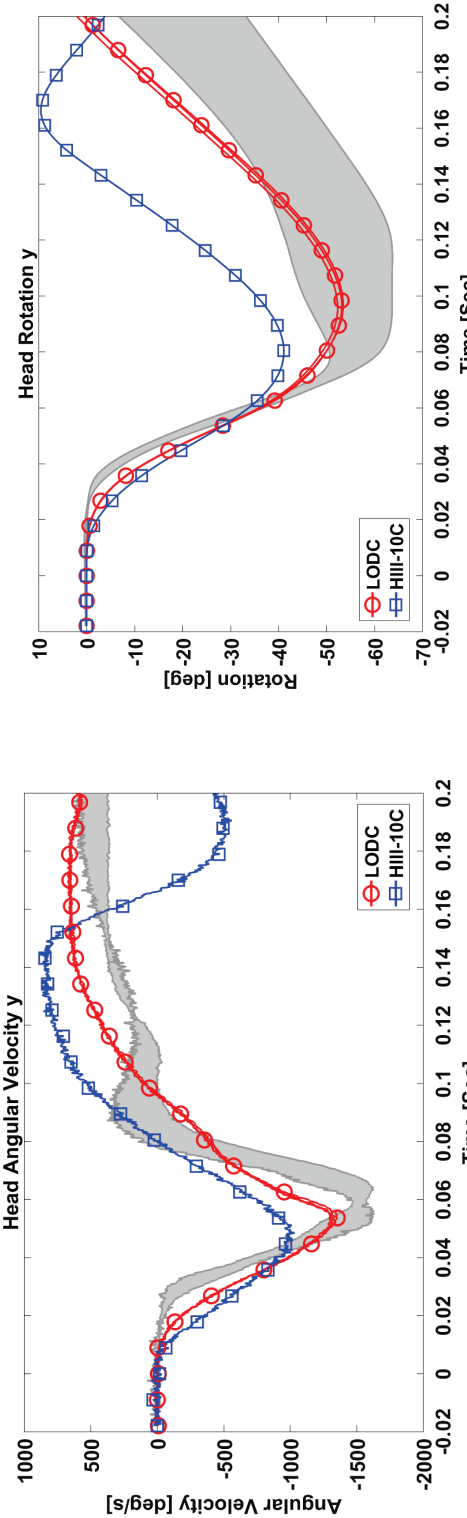

Figure 29. LODC vs. HIII-10C head angular kinematics (gray shaded = scaled PMHS)

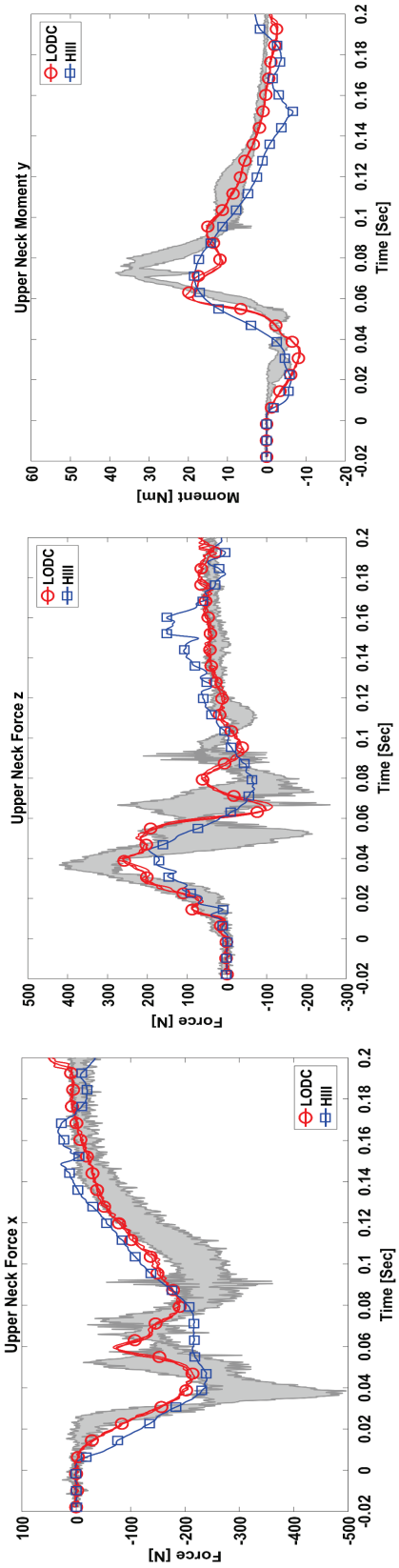

Figure 30. LODC vs. HIII-10C upper neck loads (gray shaded = scaled PMHS)

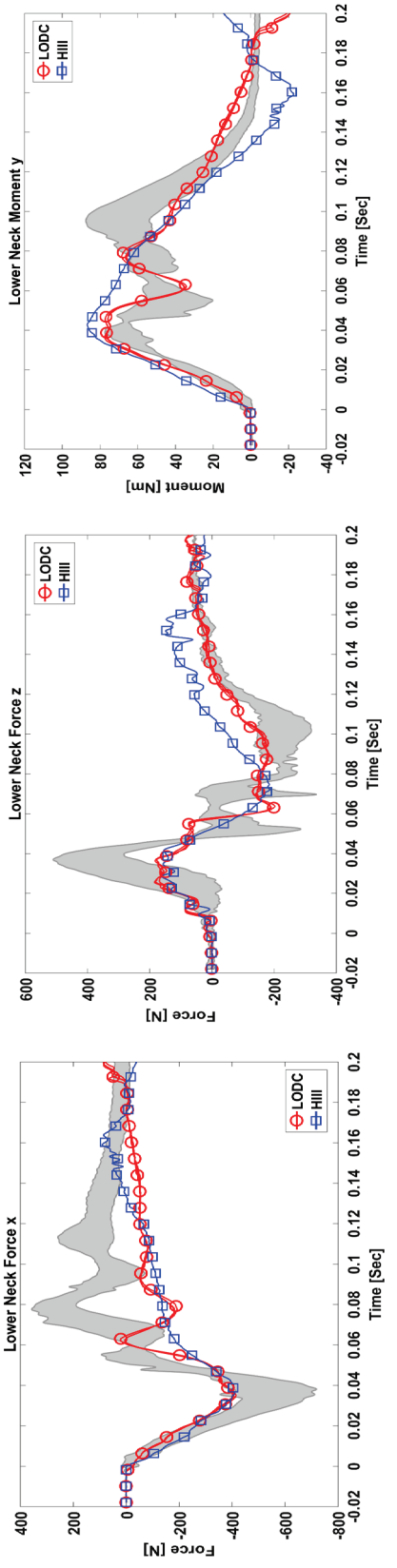

Figure 31. LODC vs. HIII-10C lower neck loads (gray shaded = scaled PMHS)

A lower neck Y moment vs. head rotation biofidelity target was created using the ellipse method from Shaw et al. (2006). Figure 32 shows how the LODC follows the corridor more closely than the HIII-10C. The peak head rotation falls near the mean of the target, while the HIII-10C rotation stops at just over 40 degrees.

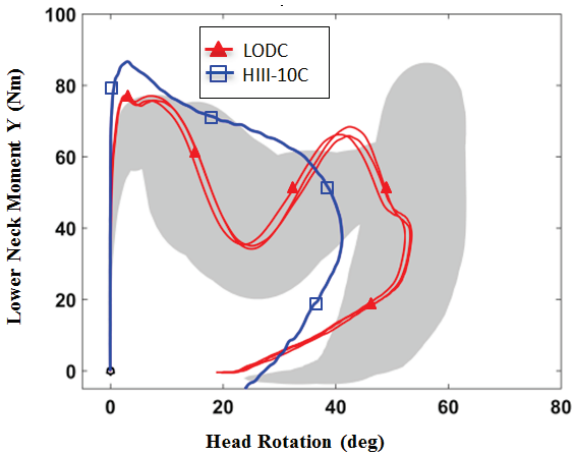

Figure 32. LODC vs. HIII-10C rotational stiffness (gray shaded = scaled PMHS)

Table 7 summarizes the BioRank scores. For the cervicothoracic test condition, the BioRank scoring was a hybrid between the corridor-based (moment vs. head rotation shown in Figure 32) and time-history based (Figures 28-31) calculation methods. The difference in upper and lower neck load scores between ATDs do not exceed the 0.2 threshold used to determine significance using BioRank, which is likely due to the rigid, non-rotating T3 boundary condition, similar ATD head-neck masses, and relatively low energy test condition (184 J). However, the head kinematics (1.19 for LODC vs. 1.92 for HIII-10C) and the lower neck Y moment with respect to head rotation (1.15 for LODC vs. 2.46 for HIII-10C) are significantly improved for the LODC in this test condition. Unlike the other four body region test conditions, this test condition utilizes scaling of adult PMHS data, so it cannot be considered a direct pediatric biofidelity assessment like the other body region test conditions. However, this test does reveal how improvements to the head mass distribution, neck response, and addition of a flexible thoracic joint contributes to more biofidelic head kinematics and overall head-neck response in the LODC.

Table 7. BioRank scores for LODC and HIII-10C cervicothoracic mini-sled tests

Measurement	LODC	HIII-10C
Head X Acceleration (g)	0.88	0.95
Head Z Acceleration (g)	0.99	1.55
Head Angular Velocity (deg/s)	1.70	2.86
Head Rotation (deg)	1.30	2.90
AVERAGE HEAD SCORE	**1.19**	**1.92**
Upper Neck X Force (N)	1.11	1.23
Upper Neck Z Force (N)	0.91	1.37
Upper Neck Y Moment (Nm)	2.22	1.77
AVERAGE UPPER NECK SCORE	**1.41**	**1.46**
Lower Neck X Force (N)	1.62	1.22
Lower Neck Z Force (N)	1.61	1.28
Lower Neck Y Moment (Nm)	1.72	1.93
AVERAGE LOWER NECK SCORE	**1.65**	**1.47**
ROTATIONAL STIFFNESS SCORE	**1.15**	**2.46**
AVERAGE CERVICOTHORACIC SCORE	**1.35**	**1.83**

Thorax. Figure 33 shows the repeatability of the LODC thorax impact response. The results from the ATD tests versus the biofidelity corridor are shown in Figure 34. The LODC was observed to have significantly greater peak deflection (76 mm) than the HIII-10C (40 mm). The HIII-10C meets the qualification corridor documented in CFR 49 Part 572, Subpart T, which is much stiffer than the new corridor specified in this analysis; therefore, it is not surprising the two ATDs display large differences in response.

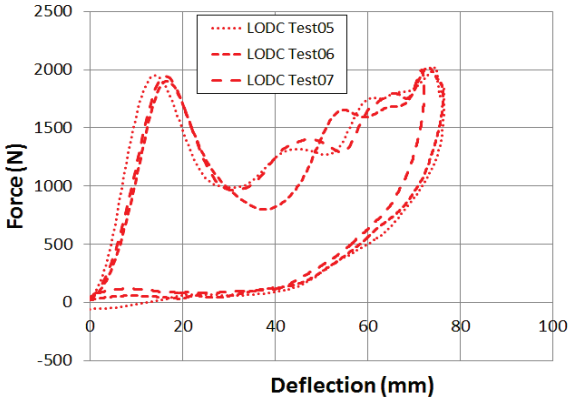

Figure 33. LODC thorax test repeatability

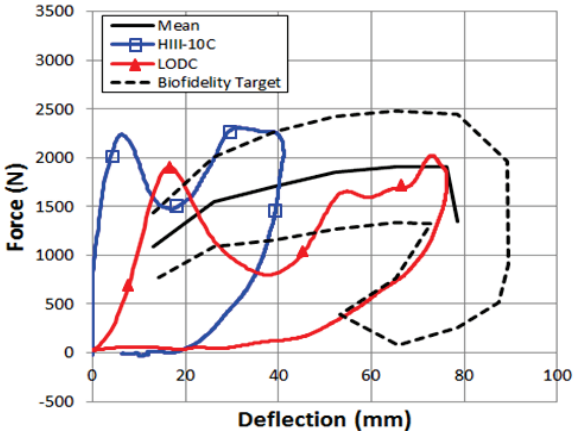

Figure 34. LODC vs. HIII-10C average response compared to biofidelity corridor

Figure 35 shows the LODC and HIII-10C mean force and mean deflection time histories versus their respective biofidelity targets.

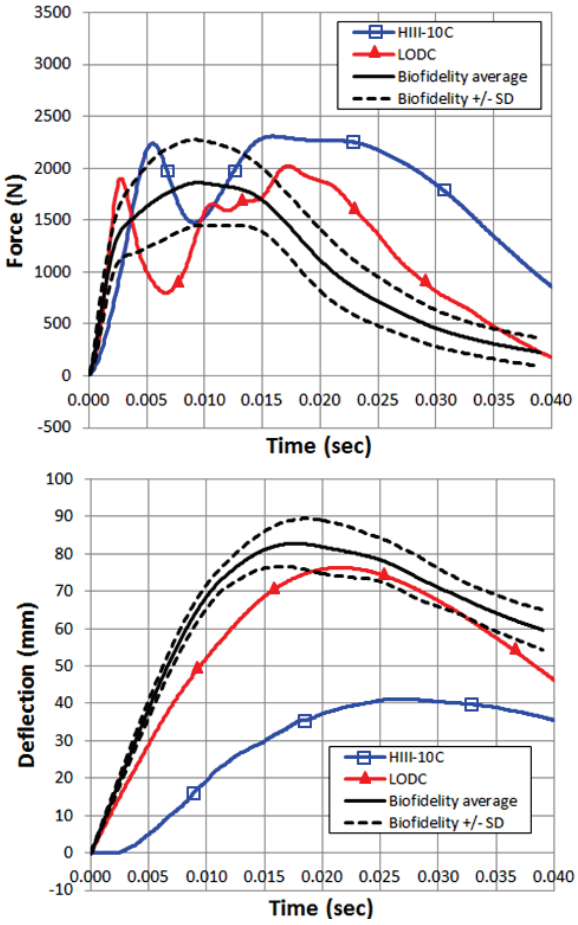

Figure 35. HIII-10C and LODC force and deflection time histories for BioRank scoring

For the thorax, BioRank scores were calculated from the mean ATD force and deflection time history data with respect to the thorax biofidelity target. The two scores were then averaged to obtain the overall thorax score (Table 8). The LODC exhibited improved thorax response biofidelity from the HIII-10C.

Table 8. BioRank scores for LODC and HIII-10C in thorax impact tests

Measurement	LODC	HIII-10C
Force vs. Time	1.79	3.17
Deflection vs. Time	1.88	7.83
AVERAGE THORAX SCORE	**1.84**	**5.50**

Abdomen. Figure 36 shows that the LODC abdomen response is repeatable in this test condition. The LODC response is closer to the mean of the corridor, as it only departs slightly from the upper bound of the target corridor from 13 – 22 mm of penetration (Figure 37), whereas the HIII-10C response is too stiff throughout the response beginning at 8 mm.

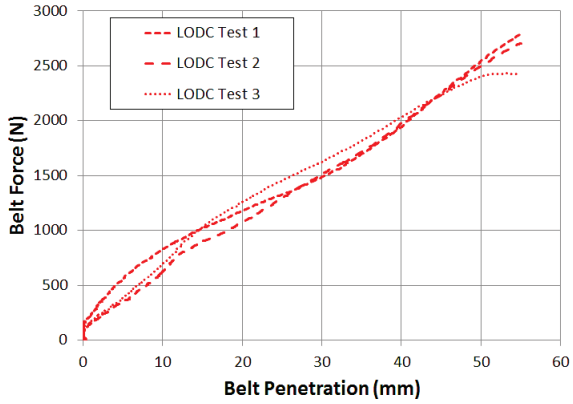

Figure 36. LODC abdomen test repeatability

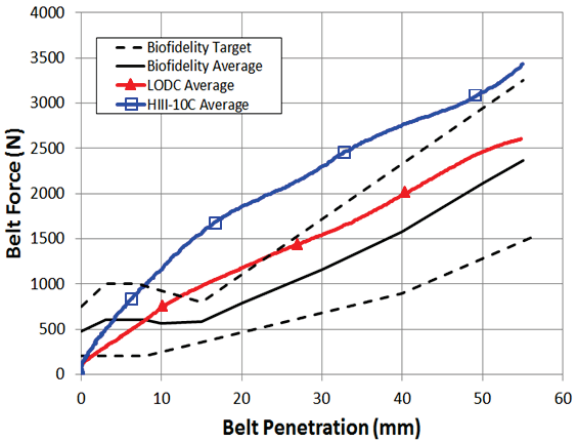

Figure 37. LODC abdomen belt pull results

Like for the neck, BioRank scores were calculated by summing the difference between the respective ATD forces and the biofidelity average at each belt penetration increment. The LODC response was found to be more consistent with the pediatric biofidelity target than the HIII-10C (Table 9).

Table 9. BioRank scores for LODC and HIII-10C abdomen tests

Measurement	Formula*	LODC	HIII-10C
TOTAL ABDOMEN BIOFIDELITY SCORE	$\sqrt{\frac{\sum(F(d_i)_{ATD} - F(d_i)_{human})^2}{\sum(\sigma(d_i)_{human})^2}}$	**0.66**	**1.61**

*$F(d_i)_{ATD}$ = ATD force at a given belt penetration, $F(d_i)_{human}$= mean human force at a given belt penetration, and $\sigma(d_i)_{human}$= human standard deviation in force at a given belt penetration

Body Region Biofidelity: Summary

Body region testing showed that the LODC has improved biofidelity over the HIII-10C when compared to biomechanical data for all body regions (Table 10). The body region BioRank scores for the LODC ranged from 0.61 for the head to 1.84 for the neck. The HIII-10C ranged from 1.61 for abdomen to 5.50 in thorax. While it is certainly possible that the difference in overall BioRank score could change if different or additional test conditions are considered, this analysis indicates that the LODC as currently constructed exhibits improved responses relative to the HIII-10C with respect to pediatric biomechanical information. The next step is to determine whether or not these improvements in body region response translate to full body kinematic improvements when evaluating restraints.

Table 10. BioRank Score Summary

Body Region	LODC	HIII-10C
Head	0.61	1.81
Neck	1.57	2.73
Cervicothoracic	1.35	1.83
Thorax	1.84	5.50
Abdomen	0.66	1.61
OVERALL ATD	**1.21**	**2.70**

FULL ATD KINEMATIC BIOFIDELITY

The second objective of this study was to assess LODC and HIII-10C full body biofidelity by comparing with the kinematics of a 13 year old PMHS (Kallieris et al. 1976). This PMHS test was previously reconstructed by both Ash et al. (2009) and Abdelilah et al. (2007) with Hybrid III child ATDs. Reconstruction information from those two studies was used to develop a sled test configuration for comparing both the LODC and HIII-10C with the PMHS data.

Methodology

Test setup. In order to reconstruct the PMHS test, the shoulder and lap belt anchorage locations were adjusted on the updated FMVSS No. 213 bench to the anchorage locations of the PMHS configuration (Table 11). In addition, belt routing for the ATDs was matched as closely as possible to the PMHS pre-test photographs, in the absence of positioning measurements from the PMHS test (Figure 38). In addition to matching the restraint configuration and belt routing, the sled pulse was replicated (Figure 39). Following the test, the Hybrid III 10 year old results were compared to results from Ash et al (2009) to assure that using the FMVSS No. 213 bench with modified belt anchorage locations was a valid representation of the PMHS test condition.

Table 11. Adapted FMVSS No. 213 bench[1] vs. PMHS configuration

Seat Parameter	PMHS Configuration	Adapted FMVSS No. 213 Bench Configuration
Seatback angle, deg	25	23
Shoulder belt anchor (X from 50th H-point), mm	-395	-398
Shoulder belt anchor (Y from seat centerline), mm	±244	±246
Shoulder belt anchor (Z from 50th H-point), mm	625	624
Lap belt anchor (X from 50th H-point), mm	-235	-233
Lap belt anchor (Y from seat centerline), mm	±300	±304
Lap belt anchor (Z from 50th H-point), mm	-235	-231

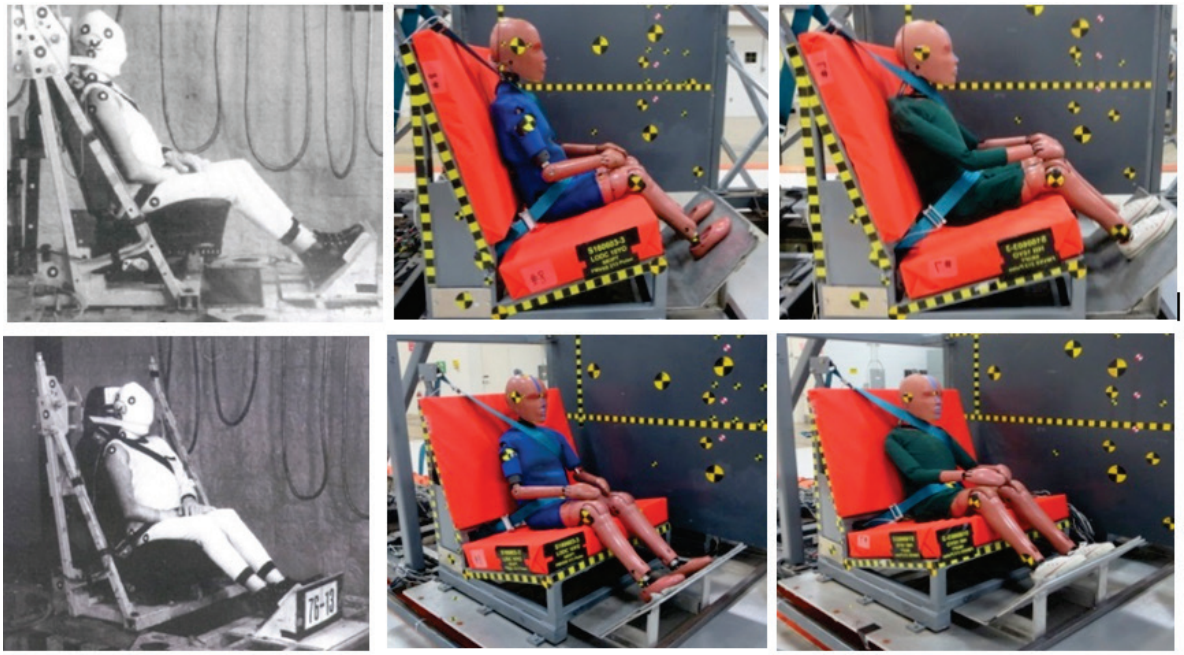

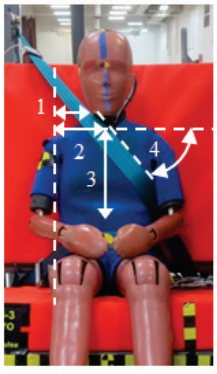

	Location	LODC	HIII-10C
1	Horizontal distance between torso outboard shoulder and first belt contact with chest (mm)	98	126
2	Horizontal distance between torso outboard shoulder and belt contact at chest centerline (mm)	155	189
3	Vertical distance between belt contact at dummy thorax centerline and lap belt contact at pelvis centerline (mm)	233	228
4	Shoulder belt angle (deg)	47	41

Figure 38. ATD positioning to match pediatric PMHS from Kallieris et al. (1976)

[1] For more details on the updated FMVSS No. 213 bench, see NHTSA-2013-0055-0002 at www.regulations.gov.

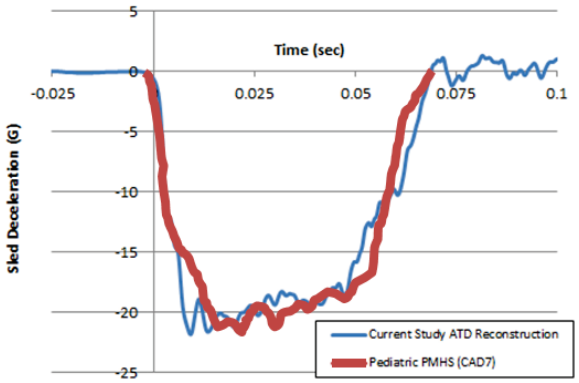

Figure 39. Pulse comparison

Instrumentation and Data Processing. Both the LODC and HIII-10C were instrumented at the head, spine, and pelvis with 3aω motion packages. The HIII-10C spine instrumentation was located at the standard location in the spine box for calculating the chest resultant acceleration 3 millisecond clip in FMVSS No. 213 tests. The LODC contained 3aω instrumentation at the T1, T6, and T12 locations at the spine (Figure 40). Because the HIII-10C has a rigid thoracic spine box, measurements from the mid-spine were transformed to the T1 location consistent with the LODC T1 location using rigid body transformation. Chest deflection was measured by a standard potentiometer in the HIII-10C, while the LODC contained an IR-TRACC connected between the spine and sternum at the rib 3 level (Figure 41). In addition to kinematic sensors, both ATDs contained upper neck, lower neck, lumbar, and ASIS load cells. As in the component tests (see Figure 9), the LODC abdomen housed twin pressure sensors (APTS, Transpolis) and a 3aω motion package on the anterior surface. As noted in Figure 9, belt penetration was calculated by subtracting the average X component displacement of the T12 and pelvis locations from the X displacement of the anterior abdomen surface. Shoulder and lap belt tension forces were measured for both ATDs. All data from both ATDs was processed using SAE J211 polarity and filtering procedures. Kinematic analysis was done using three-dimensional high speed video analysis software (TEMA software, Image Systems Motion Analysis). Belt forces and overall kinematics from the ATDs were compared with the PMHS data.

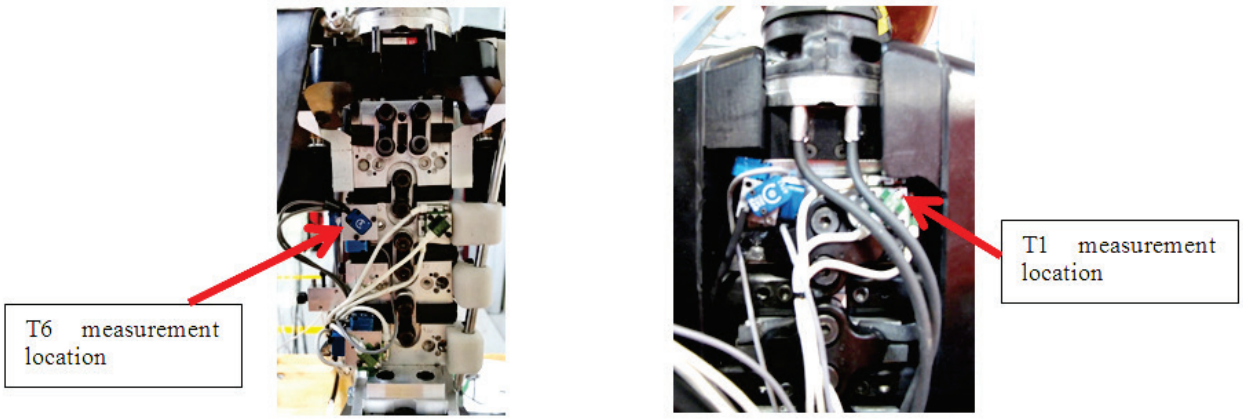

Figure 40. LODC front (left) and rear (right) chest acceleration measurement locations

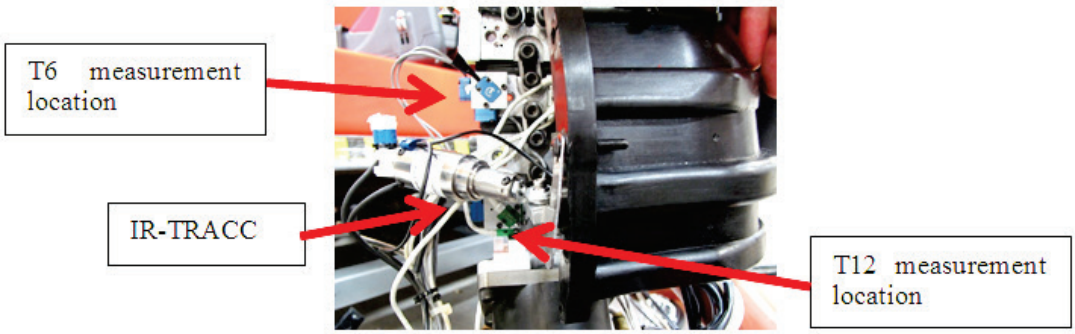

Figure 41. IR-TRACC located at rib 3 level, one spine segment below T6 instrumentation

Full Body ATD Biofidelity: Results & Discussion

With little information from the pediatric PMHS test, it was very difficult to reconstruct the test exactly with the ATDs; considerable effort was taken by previous researchers to match the exact conditions of the test. To assure reasonable accuracy, the seat belt anchorage locations and pulse were matched to the documentation, and belt positioning was matched as closely as possible to the PMHS pre-test photographs. To further assure that our test was a reasonable reconstruction, head and chest accelerations as well as belt forces were compared for the HIII-10C tests conducted by Ash et al. (2009) and the current study (Figure 42). The chest resultant accelerations were nearly identical (500 m/s^2); however, both the belt forces and head accelerations were higher in the current study than in the Ash reconstruction. This is likely due to cumulative differences in initial belt fit, head position, different ATDs, pulse, and the use of the 213 bench instead of the actual vehicle seat used for the original test. Nonetheless, for the purposes of comparing the LODC and HIII-10C in a similar condition as a rare pediatric PMHS test, it was worthwhile to assess whether the body region biofidelity improvements in the LODC translated to more biofidelic full body kinematics as well.

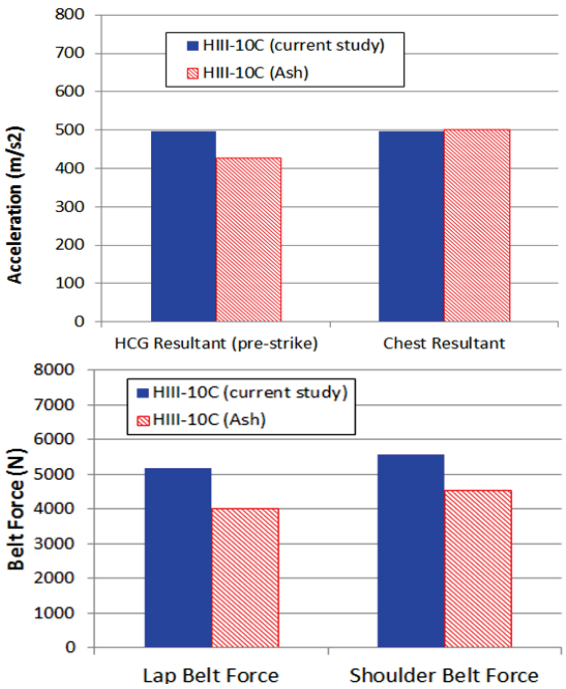

Figure 42. HIII-10C acceleration & belt force comparison between Ash & current study

Figure 43 compares the kinematics of the pediatric PMHS, LODC, and HIII-10C at various time points. The H-points for all three cohorts were set at the (0,0) position at each time point in the stick plots, which removes differences between ATD and PMHS lower body sliding, belt stretch, and foot plate interaction so that upper body kinematic similarities or differences are more easily discerned. Up to 80 ms, the LODC mimics the PMHS quite closely while the HIII-10C spine moves very little as the head rotates sooner. At 80 ms, the ATD feet lose contact with the foot rest, allowing the legs to move forward and away from the head, while the PMHS legs remain in contact as the head continues to "pocket" into the space between the chest and upper legs.

The LODC head trajectory more closely approximated the PMHS (Figure 44), both in peak forward translation as well as peak downward motion. The greater forward excursion is a direct consequence of a more flexible thoracic spine and softer thorax in the LODC than the HIII-10C. The LODC shoulder belt force was slightly (9%) higher than the PMHS shoulder belt force, while the HIII-10C force was 37% higher than the PMHS. Note that, as shown in Figure 42, the HIII-10C belt force from this test was roughly 20% greater than the HIII-10C in the original reconstruction.

The lap belt forces for the ATDs were quite similar to one another but both were 80% greater than the PMHS lap belt force. It is unclear why the PMHS lap belt forces were so much lower than the ATDs. The PMHS clearly did not submarine from the video captures and the lap belt appeared to remain on the pelvis. Four possible reasons for the lower lap belt force are that the (1) center of mass of the PMHS is higher than the ATDs, producing more upper body flexion and more sliding of the lap belt instead of compressing the pelvis, (2) the PMHS anterior pelvis is less stiff than the ATD anterior pelvis, (3) the PMHS forward motion was restrained by not only the belt but also the foot plate, and (4) differences between the original vehicle seat and FMVSS 213 bench. Given similar masses of the ATDs and PMHS, the restraint configuration used for the reconstruction, even with matched belt anchorage locations, did not adequately match the PMHS test in terms of lower body kinematics. The sums of the shoulder and lap belt forces for the PMHS and ATD did not equate given the same applied sled pulse; if the foot plate reaction force was measured and original seat were used, the ATD and PMHS total restraint forces (shoulder + lap + foot plate) would likely be more similar.

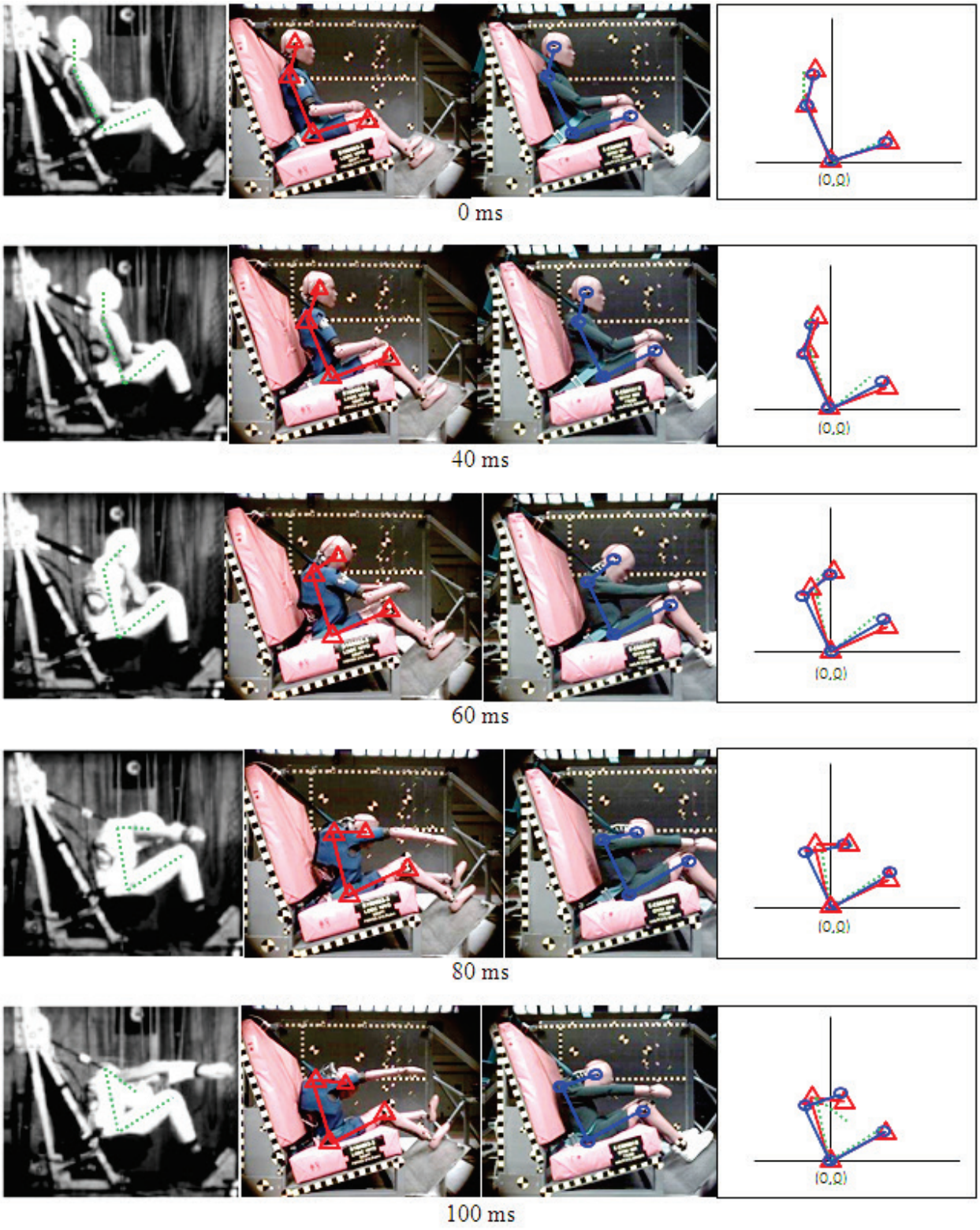

Figure 43. Kinematics of (left, green dotted) pediatric PMHS, (center, red triangle) LODC, and (right, blue circle) HIII-10C in a 40 km/h test

In terms of head acceleration, Figures 45-46 show how the LODC and HIII-10C compared with one another and with the PMHS, both overall and before the chin strikes the chest. In peak acceleration before chin impact, the LODC had lower acceleration (412 m/s^2) but HIII-10C had higher acceleration (498 m/s^2) than the PMHS (456 m/s^2). For the overall head acceleration, both the LODC (683 m/s^2) and HIII-10C (590 m/s^2) had lower head acceleration than the PMHS (720 m/s^2) in this test condition. It is interesting that the difference between pre-strike and overall acceleration was smaller for the HIII-10C (92 m/s^2) than for the LODC (271 m/s^2). In other words, the chin strike made a larger difference for the LODC than for the HIII-10C. The larger LODC difference did however more closely reflect the large difference for the PMHS (264 m/s^2).

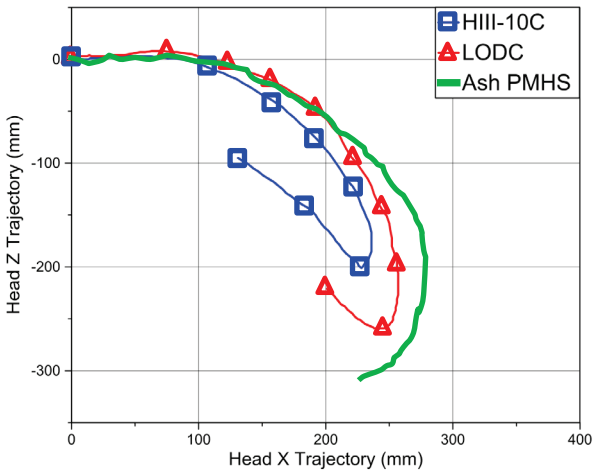

Figure 44. HIII-10C, LODC, and pediatric PMHS head kinematics

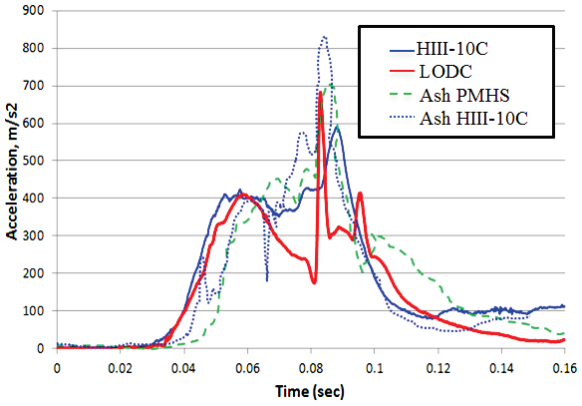

Figure 45. Head resultant accelerations of LODC, HIII-10C (this study and from Ash), and PMHS

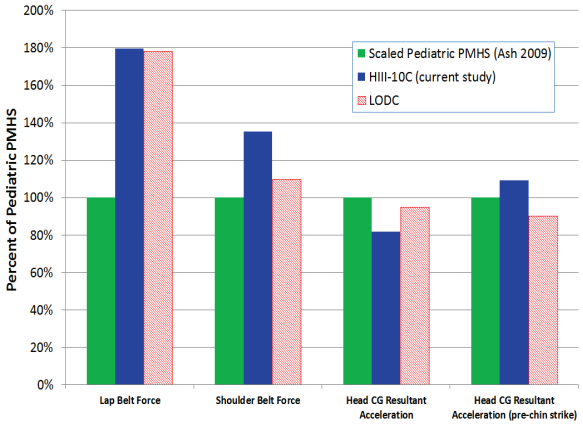

Figure 46. HIII-10C, LODC, and pediatric PMHS belt forces & head accelerations

SLED TEST COMPARISON WITH HYBRID III 10 YEAR OLD

The third objective of this study was to compare the LODC directly to the HIII-10C in FMVSS No. 213 sled testing. There were three primary focus areas for this comparison:

(1) Understand how improvements in body region biofidelity influence the full body kinematics and performance of the LODC in evaluating child restraints.

(2) Evaluate whether the LODC solves issues observed with the HIII-10C, such as chin-to-chest contact, inadequate identification of submarining, and lack of sensitivity to different types of restraint configurations.

(3) Evaluate whether the LODC, which consists of flexible and complex components, is robust enough to withstand the crash simulation scenarios such as FMVSS No. 213 that it would be used in.

Methodology

Test Setup. LODC and HIII-10C ATDs were positioned side-by-side on the updated version of the FMVSS No. 213 bench that reflects recent vehicle seat stiffness and belt anchorage locations (NHTSA 2013). Four restraint configurations appropriate for a 10 year old occupant were applied: (1) Five point harness (Britax Frontier Clicktight), (2) highback belt positioning booster (Evenflo Big Kid), (3) backless belt positioning booster (Graco Turbobooster), and (4) no CRS with a slouched posture (Figure 47). The standard FMVSS No. 213 pulse was used. The

ATDs were positioned as consistently as possible with one another, with allowable body landmark location and belt geometry differences of less than 10 mm. The test matrix is shown in Table 12.

Table 12. Test matrix to compare LODC with HIII-10C

Test #	Left Side	Right Side	CRS
1	HIII-10C	LODC	5-Pt Harness
2			Highback BPB
3			Backless BPB
4			No CRS/Slouch

*CFR 49 Part 571; 213
**NHTSA is in the process of updating the bench in FMVSS No. 213. See NHTSA-2013-0055.

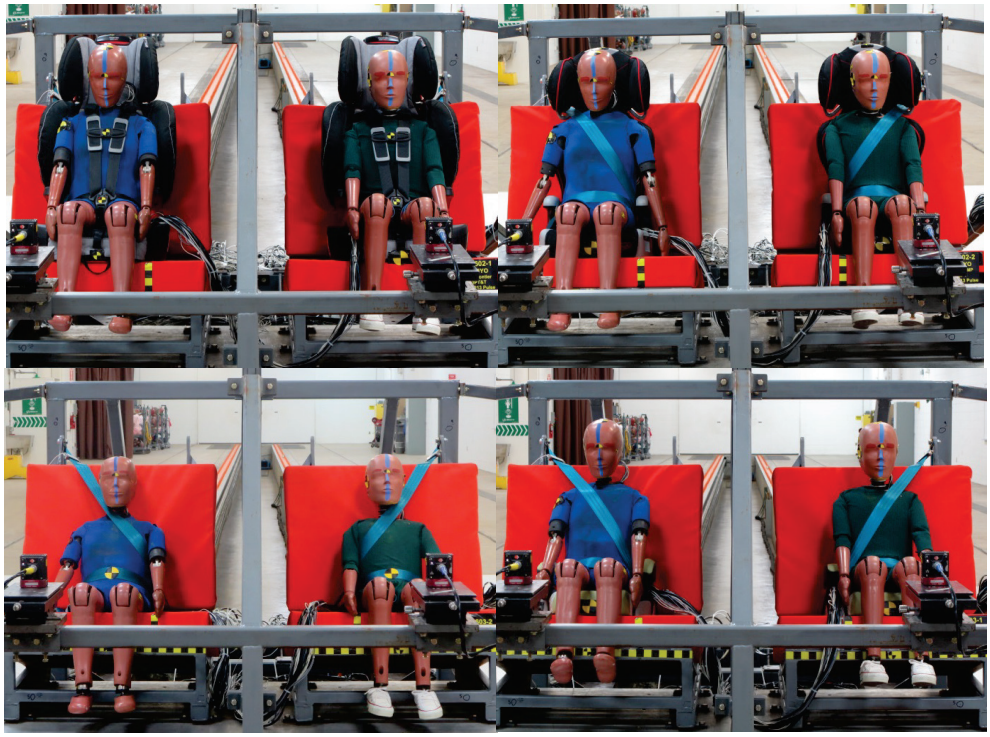

Figure 47. LODC (left) and HIII-10C (right) in four restraint configurations. Clockwise from top left: (1) 5 point harness, (2) highback booster, (3) backless booster, (4) no CRS

Instrumentation & Data Processing. Both ATDs were instrumented the same way as described in the previous section, with the same filtering and data processing methods applied to the test data. Abdominal penetration was calculated as described in Figure 9.

Results & Discussion

Kinematics.

Figure 48 shows the head trajectories of both LODC and HIII-10C in the four restraint conditions. In the booster seat cases, larger displacements were observed in LODC than in HIII-10C, both in the forward X and downward Z directions, similar to the PMHS reconstruction test. In the no CRS case, both ATDs displayed a more "narrow" trajectory than in the CRS configurations, with the LODC having slightly more forward displacement but similar downward motion. Full body kinematic diagrams for LODC and HIII-10C are found in Appendix B. The largest kinematic difference between the ATDs occurs in the 60 – 80 ms timeframe.

Chin-to-Chest Contact. HIC is not currently a criterion for the HIII-10C in FMVSS No. 213, primarily because of the discrepancy between elevated HIC values in child restraint tests and the absence of head injuries attributed to chin-to-chest contact in field data (Stammen et al. 2012a). While HIC is not an IARV for the HIII-10C nor is it intended to assess the risk of injury in non-contact conditions, it is still a useful diagnostic measure for assessing the relative severity of a chin-to-chest contact. Figure 49 shows how the head resultant spikes due to hard chin-to-chest contact in the 80 millisecond timeframe in the HIII-10C are either not present or not contributing to the HIC outcome in the LODC traces. The increased head translation, less severe head rotational velocity, and softer thorax in the LODC prevents the hard chin contacts and elevated HIC outcomes that were observed in the HIII-10C. HIC for the LODC was reduced anywhere from 10.3% for the 5-point harness to 64.3% for the highback BPB case with respect to the HIII-10C (Figure 50). The softer chin interaction with the chest results in more stable head acceleration traces, and therefore restraint design can be focused primarily on overall protection of the occupant without the impediment of how to reduce HIC in the FMVSS No. 213 test environment. It has been suggested that decreasing HIC in the FMVSS No. 213 environment when using the HIII-10C could require inadequate belt fit and increased risk of torso rollout or submarining (Klinich et al. 2008). With more realistic head accelerations when using the LODC, emphasis can be placed more on head kinematics and proper belt fit rather than trying to mitigate high acceleration spikes due to hard chin-to-chest contact. Also, chin-to-chest contact has precluded the use of the HIII-10C in the rear seat in full-scale vehicle testing; it may now be possible to evaluate head injury risk without any conditional requirements (for example, visible head contact).

Neck Loading. Aside from hard chin-to-chest contact, another limitation of the HIII-10C is that neck loads often far exceed estimated injury tolerance levels, even in ideal restraint situations. In the four test conditions in this study, upper and lower neck loads were decreased by 32.4% on average for the LODC with respect to the HIII-10C (Figure 51).

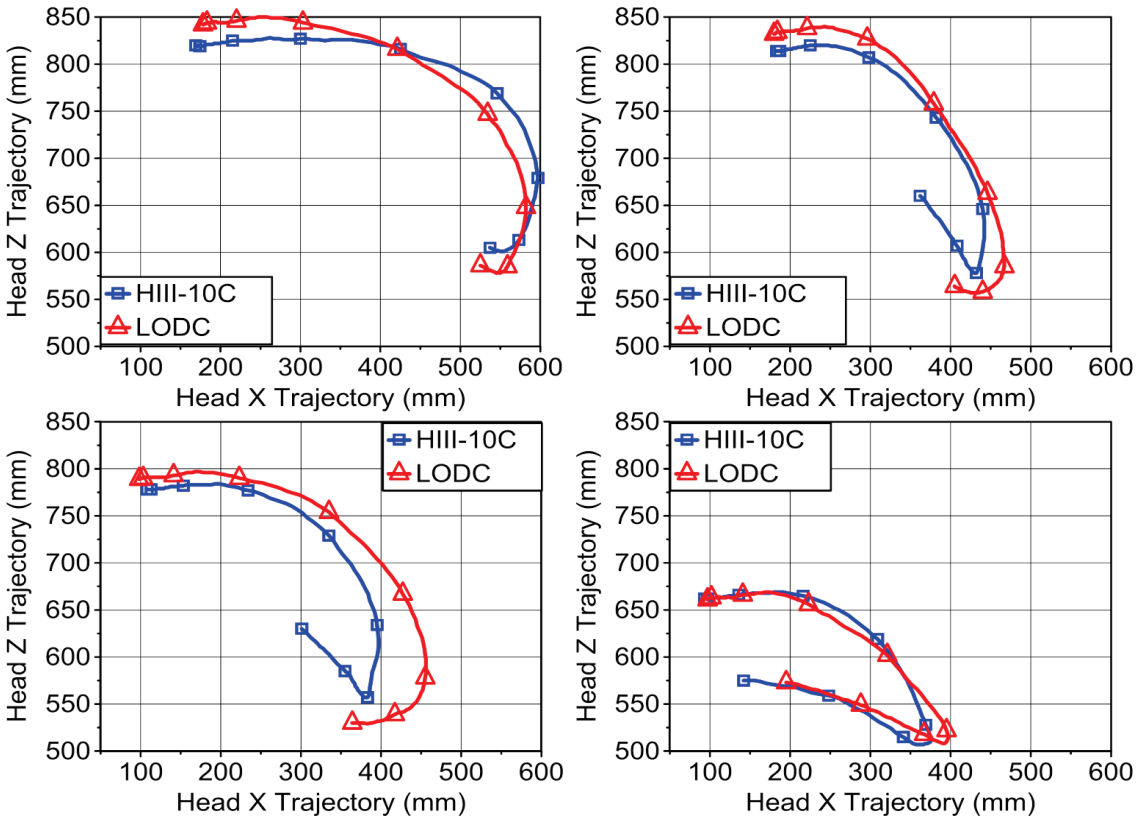

Figure 48. LODC and HIII-10C head trajectories; (clockwise from top left) 5 point harness, highback booster, no CRS, backless booster

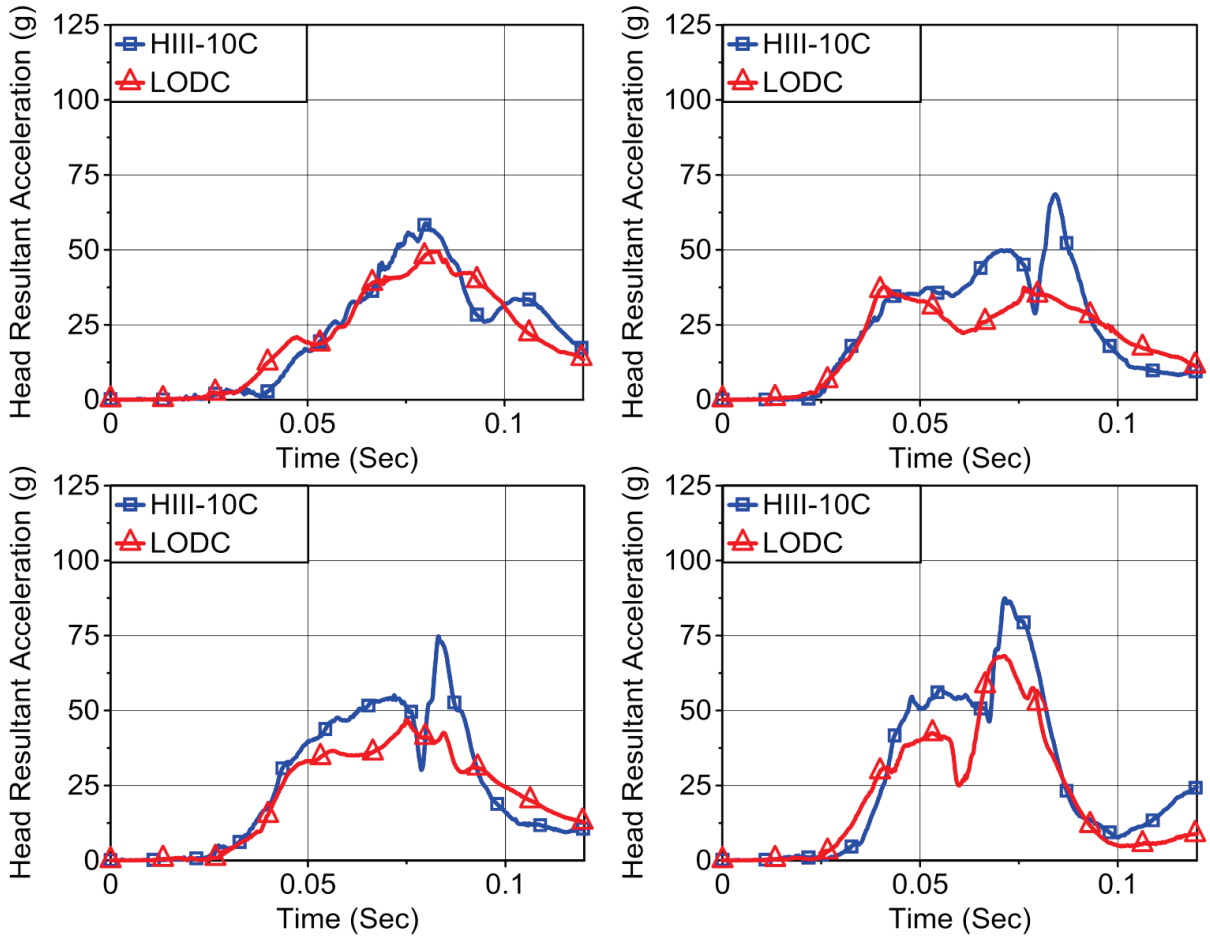

Figure 49. Head resultant acceleration vs. time for LODC and HIII-10C; (clockwise from top left) 5 point harness, highback booster, no CRS, backless booster

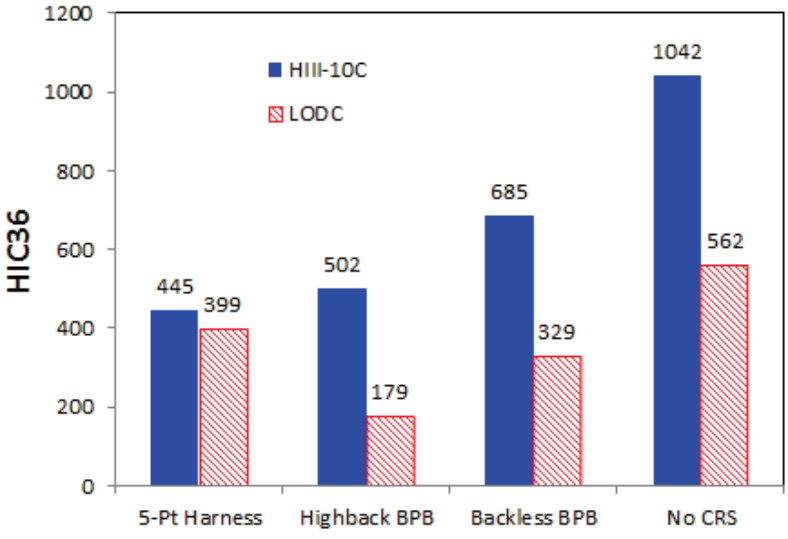

HIC Time Intervals (in milliseconds)

Restraint	HIII-10C	LODC
5-Pt Harness	59 - 95	63 - 99
Highback BPB	55 - 91	63 - 99
Backless BPB	54 - 90	51 - 87
No CRS	46 - 82	46 - 82

Figure 50. HIC 36 comparison between HIII-10C and LODC, with time intervals for both ATDs

The greatest reductions were in the lower neck FX (58.6%) and lower neck MY (61.5%) channels. Twenty-one of the 24 total channels across the four restraint conditions were decreased in the LODC in comparison to the HIII-10C. There were three instances where the LODC actually had higher axial forces than the HIII-10C. The upper neck FZ (20.6%) and lower neck FZ (8.5%) in the 5-pt harness, as well as the lower neck FZ in the no CRS case (22.1%) were all higher in the LODC. The LODC upper neck axial forces in the three booster seat tests in particular were all 2200 N or lower, while the HIII-10C had a considerably higher upper neck FZ of 3260 N in the backless booster case. The lower magnitude LODC neck forces in the three booster seat cases could indicate that assessment of neck injury risk may be more accurate with the LODC than with the HIII-10C, in terms of discriminating between restraint situations not expected to result in neck injuries (booster cases) and those restraint situations more likely to result in neck trauma due to occupant submarining (no CRS/slouch case). However, the HIII-10C also exhibited higher neck loads in the no CRS/slouch case than it did in the booster seat cases. While the LODC tended to display lower magnitude neck loads, more study is needed to determine whether the LODC can more accurately identify neck injury scenarios than HIII-10C.

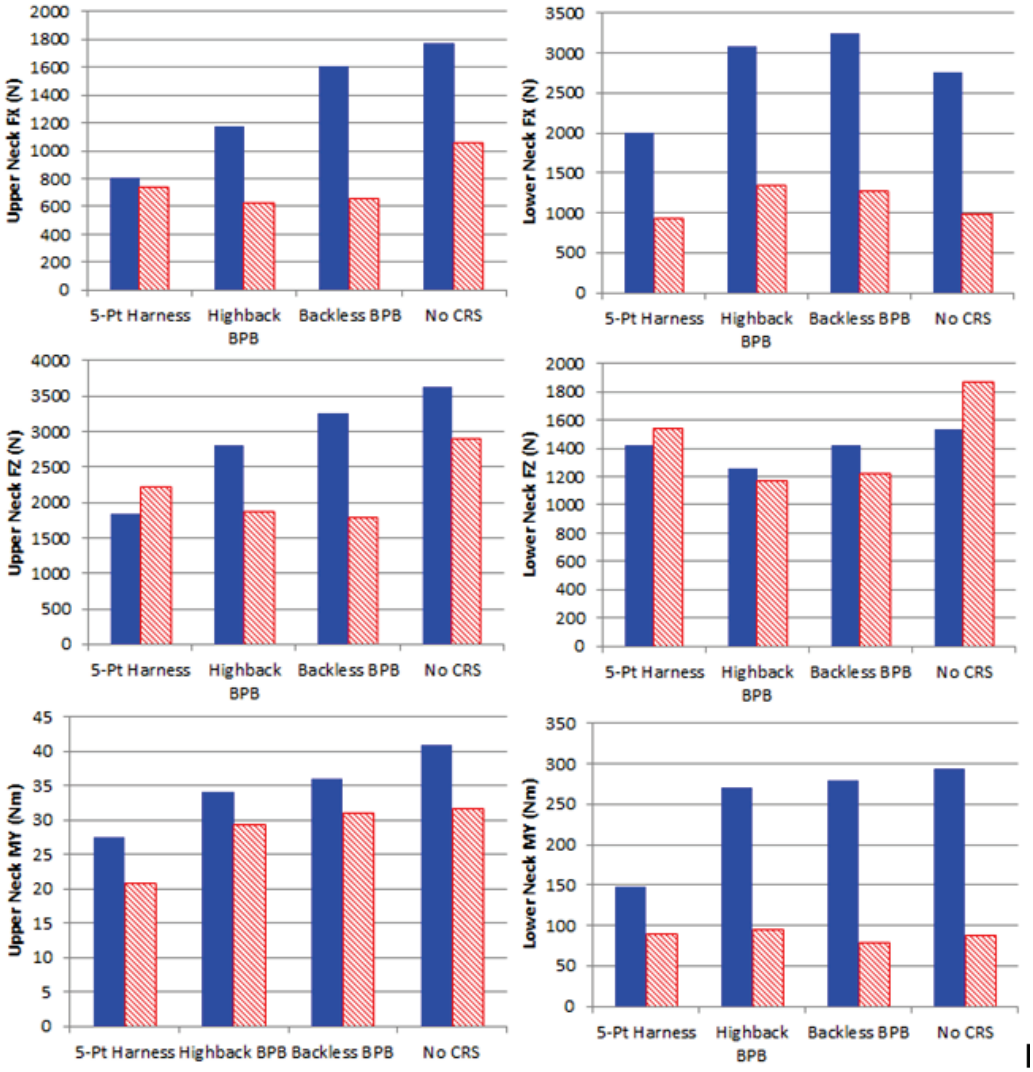

Figure 51. Neck loads for HIII-10C (solid) and LODC (hashed) in 4 restraint conditions

FMVSS No. 213 IARV. Table 13 summarizes the differences in chest acceleration, head excursion, and knee excursion for the two ATDs. There was little difference in knee excursion between the two ATDs. The backless booster and 5 point harness cases showed large increases in head excursion for the LODC. As shown earlier (see Figure 40), the LODC has two chest acceleration measurement locations on the spine while the HIII-10C measures acceleration at only one location within the area encompassed by the two LODC sensor locations. The LODC chest accelerations were lower in all four restraint conditions than for the HIII-10C, with the HIII-10C doing best with the harness and worst with the backless booster and the LODC ranking the backless booster best and no CRS case worst. Measuring acceleration at multiple locations along the spine is advantageous because more data is available for determining the optimal shoulder belt fit. For example, in the CRS cases, the T6 location had higher acceleration than T1 while in the no CRS case, the T1 acceleration was higher than T6.

Belt Forces. Figure 52 shows that the LODC shoulder belt forces were lower than the HIII-10C forces in all cases except the 5-point harness case, where the force noted is that of the vehicle belt holding the CRS to the FMVSS No. 213 test bench. This may be due in part to the mass distribution difference between the dummies. Table 2 shows that the LODC upper torso is lighter while the lower torso is heavier than the HIII-10C. It appears the lighter upper torso mass coupled with the softer ribcage in the LODC results in lower shoulder belt loads.

Table 13. Comparison of FMVSS No. 213 IARV for LODC vs. HIII-10C

Restraint	Chest Acceleration, 3 ms resultant clip (G)		Head Excursion (mm)		Knee Excursion (mm)	
	HIII-10C	LODC (T1/T6/avg)	HIII-10C	LODC	HIII-10C	LODC
5 Pt Harness	41.7	37.8/42.3/40.1	713	804	833	828
Highback BPB	44.7	33.7/39.8/36.8	550	560	703	722
Backless BPB	47.2	33.0/39.8/36.4	494	608	688	695
No CRS/Slouched	42.7	42.6/40.4/41.5	464	462	861	830

For the lap belt forces, the LODC and HIII-10C were consistent in the 5-point harness case (Figure 53). In the booster seat cases, the LODC lap belt forces were higher than the HIII-10C, which is likely due to the heavier lower body of the LODC. In the no CRS/slouch case, the softer abdomen contributed to the much lower LODC lap belt force.

Chest Deflection. The LODC thorax is much softer than the HIII-10C thorax (see Figure 34 for component responses), but the difference in chest deflections between the dummies was not as dramatic in the sled tests. The deflections were very consistent for the two ATDs in the booster seat cases (Figure 54). The LODC deflection was slightly higher (36 mm) than the HIII-10C deflection (34 mm) in the highback BPB case and slightly lower (30 vs. 31 mm) in the backless BPB case. In the no CRS case, the LODC displayed a signficantly higher (32.5 vs. 15.5 mm) displacement than the HIII-10C. There was an IR-TRACC potentiometer failure in the 5-point harness case for the LODC, so only the HIII-10C chest deflection (12.5 mm) is shown. It is expected that for the relatively benign harness case, the LODC would have experienced a low deflection similar to the HIII-10C. With similar deflections measured by the LODC and HIII-10C in the CRS cases, the focus is therefore on the worst case situation for the occupant (no CRS) where the shoulder belt position is less controlled. The much higher deflection in the LODC in the no CRS case is likely due to both a slight difference between the HIII-10C potentiometer and LODC IR-TRACC locations within the ribcage and the LODC flexible spine creating a time-varying posterior boundary condition for the IR-TRACC. The IR-TRACC is located at the rib 3 level, which is one spine segment below the T6 spine instrumentation so that it would not interfere with the spine upon ribcage compression (see Figure 41). However, it appears that the LODC thorax takes a long time to recover (deflection traces continue to be much greater than zero at 150 ms). It is suspected that this is due to the IR-TRACC either interfering with spine instrumentation as the spine is flexing, or the IR-TRACC is binding on rebound. More work is needed to investigate how to more efficiently package the spine instrumentation and IR-TRACC together within the LODC chest as it is loaded by the shoulder belt. Also, more testing is required to understand how to effectively identify and measure the maximum deflection experienced by the LODC. This may require multi-point measurement, if packaging allows for multiple deflection sensors.

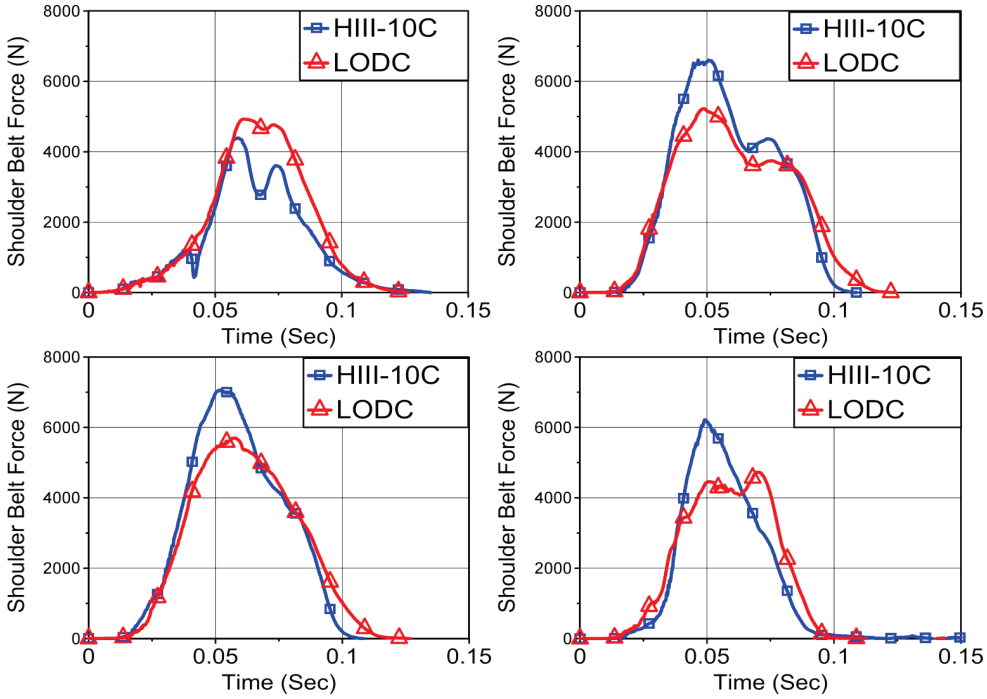

Figure 52. Shoulder belt force time histories. In the harness test, the force shown is that of the shoulder portion of the vehicle belt holding the CRS to the FMVSS No. 213 test bench.

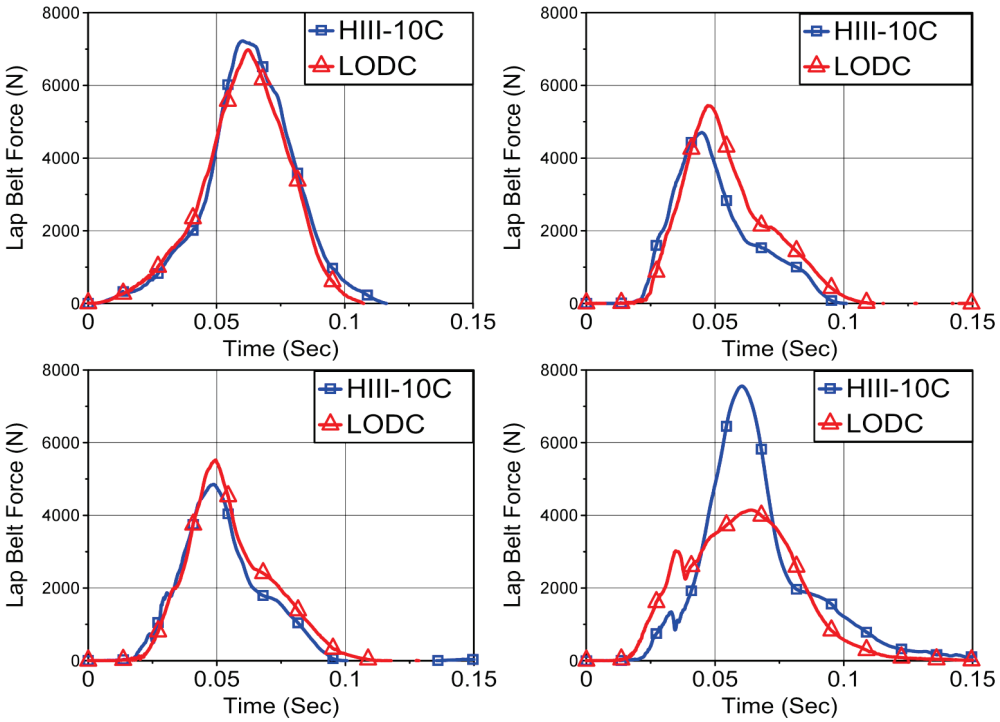

Figure 53. Lap belt force time histories. In the harness test, the force shown is that of the lap portion of the vehicle belt holding the CRS to the FMVSS No. 213 test bench.

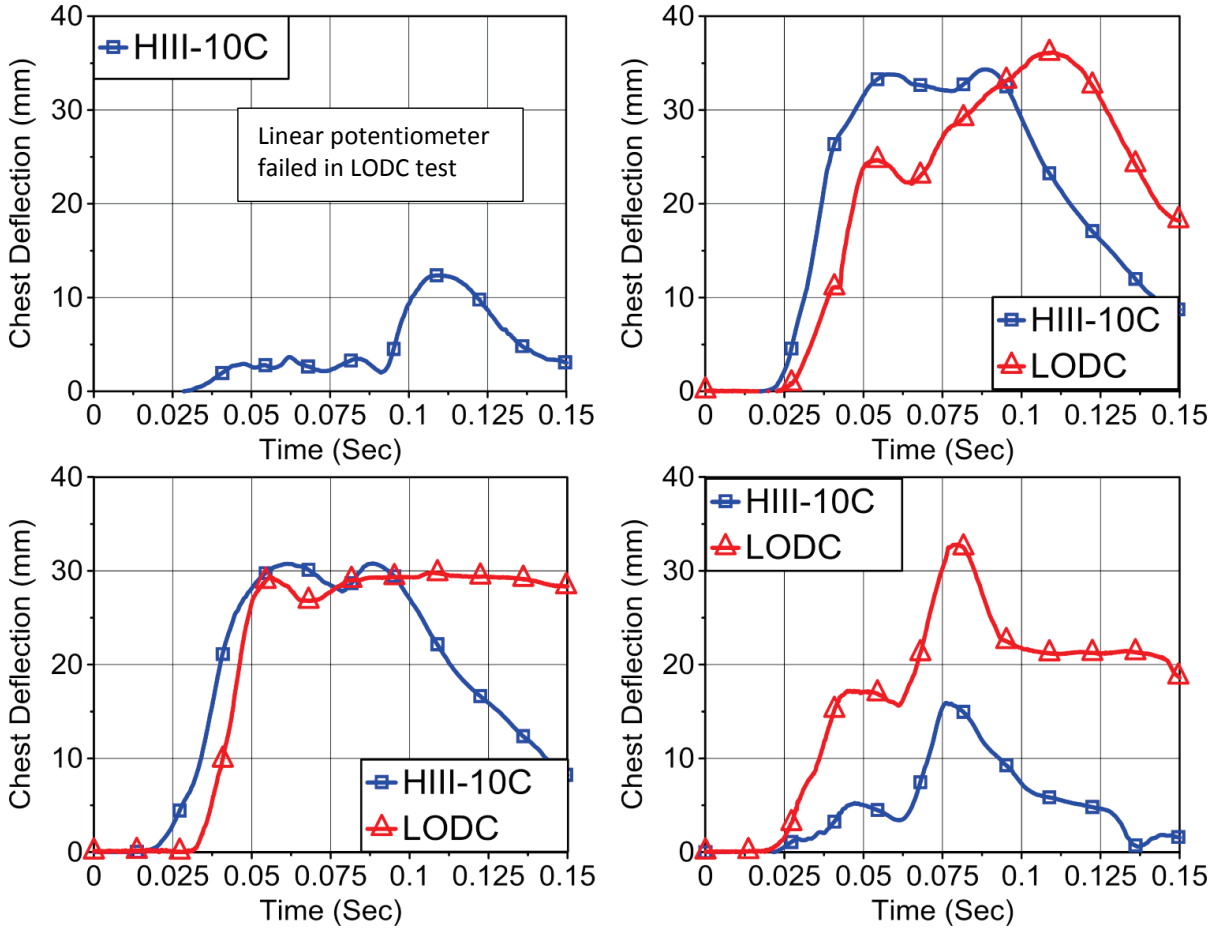

Figure 54. Chest deflections for HIII-10C and LODC

Abdominal Loading. Since there is no abdominal instrumentation in the HIII-10C, it is not feasible to compare abdominal pressure of the LODC and HIII-10C. There was a dramatic increase in LODC abdomen pressure in the no CRS condition from the child restraint conditions, as both the LODC and HIII-10C clearly exhibited submarining according to high speed video in the no CRS case (Figure 55). Since the time derivative of pressure has been suggested as an abdominal injury measure (Kremer et al. 2011), Figure 56 shows how the Pdot time histories varied by restraint condition.

While pressure is the primary measure for abdomen injury assessment, abdomen penetration was also calculated in the LODC. Because this parameter was calculated using integration of 3aω accelerometer and ARS data from the pelvis, T12, and abdomen front surface locations where any of those displacements could change direction independently of one another, penetration is reported at the time of maximum belt force (Figure 57, Table 14). In this test series, the LODC abdomen penetrations clearly distinguished between good and poor lap belt loading configurations, with the child restraint tests having 4% or less compression while the no CRS case with the lap belt over the umbilicus area showed 50.5% compression. However, penetration should be considered only an estimate at this time given the assumption that the belt is moving in plane with the average of the pelvis and T12 motion even though the lumbar joint is bending. While further development work is necessary, penetration may become a viable supplement to pressure in monitoring overall abdomen injury risk in the LODC.

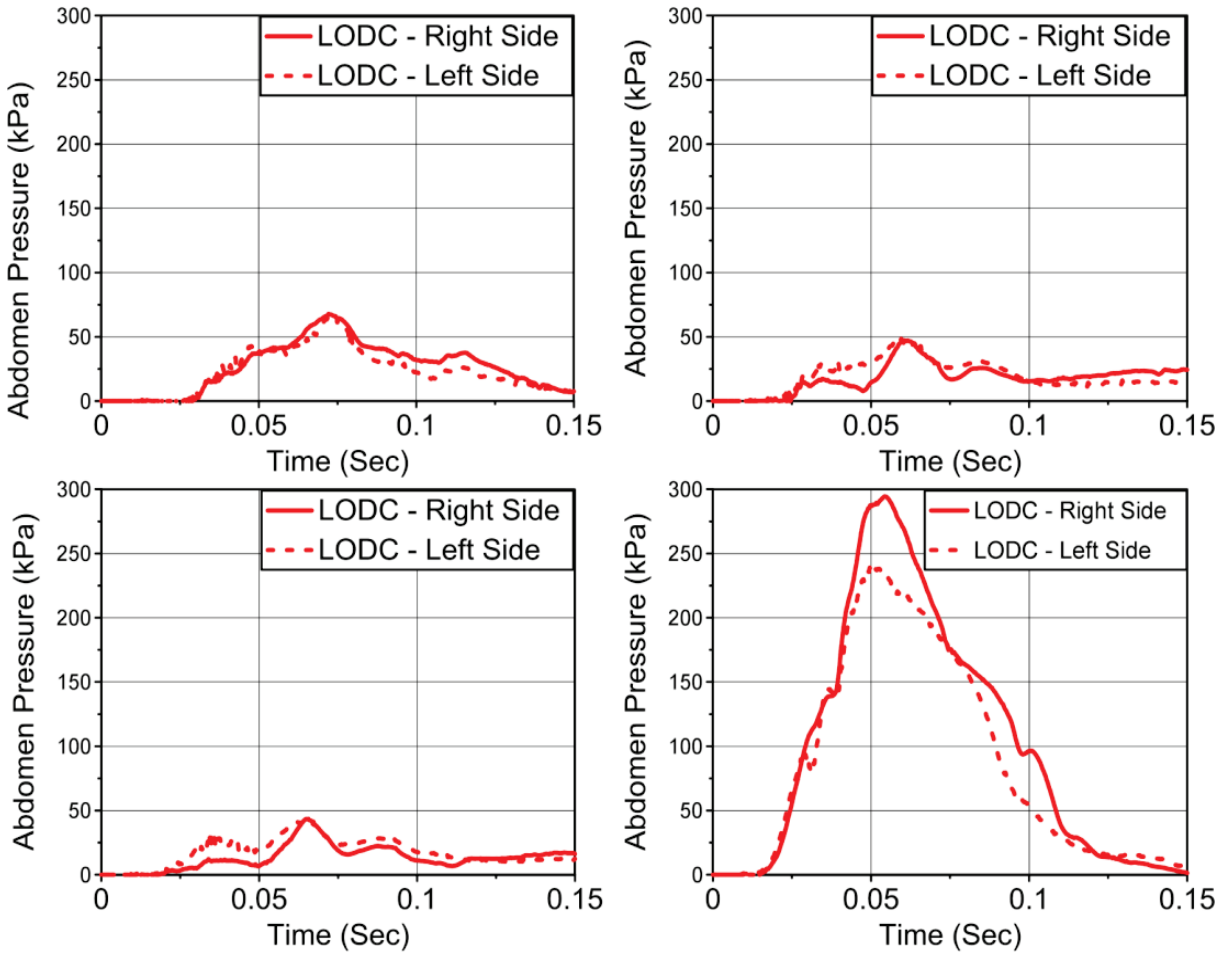

Figure 55. Pressure-time histories in LODC abdomen for 4 restraint conditions

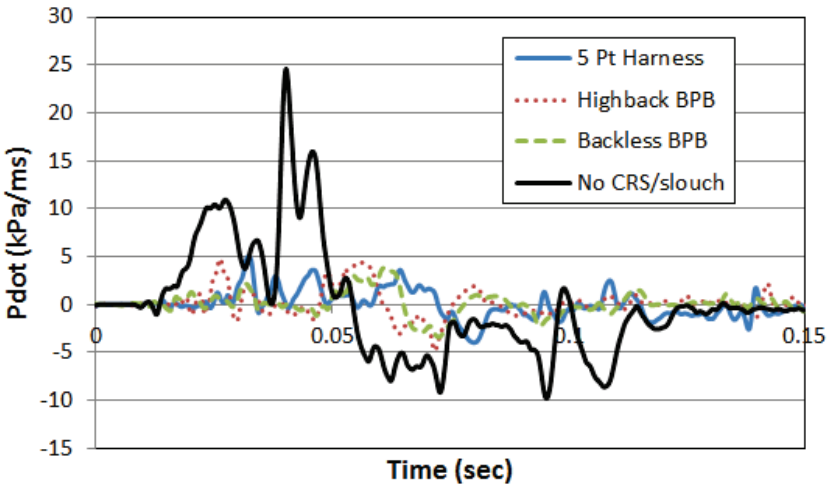

Figure 56. LODC abdomen Pdot time histories

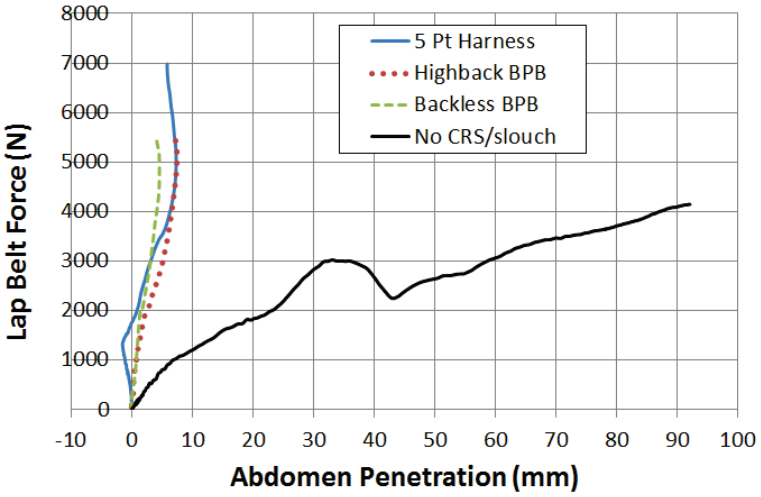

Figure 57. Lap belt force versus abdomen penetration

Table 14. LODC abdomen measurements

Restraint	Peak pressure, avg left/right (kPa)	Peak lap belt force (N)	Penetration at peak lap belt force (mm)	Pdot (kPa/ms)
5 Pt Harness	67.0	6981	5.9	5.0
Highback BPB	47.9	5445	7.2	4.8
Backless BPB	43.4	5521	3.6	3.9
No CRS/Slouch	267.0	4144	92.6	24.6

DURABILITY AND REPRODUCIBILITY

While the primary focus of this study was on biofidelity, comparison with the HIII-10C, and to a lesser extent, repeatability, there are other aspects of an ATD design that are important in its overall acceptance as a viable tool. Making an ATD more biofidelic requires more moving joints, more complex parts, and softer materials. Implementing parts with these characteristics tends to degrade both durability and repeatability. Evaluations of earlier build levels of the LODC resulted in delamination, tearing, and other damage that made the ATD unsuitable for testing. The LODC design has been gradually made more robust so that now the primary focus areas are improving its instrumentation and usability. No catastrophic damage or failures of the ATD itself occurred in this evaluation. Some wear was evident in the softest parts, such as the abdomen, thoracic spine rubber elements, and neck nodding blocks. But repeatability was maintained even with this wear. Reproducibility has not yet been assessed; it will be evaluated once the LODC design is frozen and multiple LODC ATDs are built according to those specifications. There are also plans to share the LODC with other users, so that experience can be gained and feedback can be leveraged to improve the ATD design further.

LIMITATIONS

In the evaluation of both body region and full body biofidelity of the ATDs, many of the test conditions were similar but not identical to previous pediatric tests. In the neck test, the ATDs were compared to pediatric model data from Dibb et al. 2014 rather than directly to pediatric experimental test data. In the thorax test, the corridor was scaled from pediatric experimental data from Ouyang et al. 2006. In the abdomen tests, the ATD setup consisted of a seated upright position rather than the supine position used by Kent et al. (2006) to generate the pediatric target. The cervicothoracic test was done using adult PMHS (Kang et al. 2016), with the data scaled to a 10 year old size. For the full ATD comparison, the PMHS data was obtained from publications where the PMHS test was reconstructed (Ash et al. 2009, Abdelilah 2009) because there was not enough information available that provided detailed documentation of the PMHS test itself. Despite these

discrepancies between pediatric and ATD test conditions, it is believed that this battery of tests to compare the LODC and HIII-10C provides the best possible assessment given the pediatric data available. Another limitation of this study is the very small number of sled tests used to compare the LODC with the HIII-10C. Once the chest deflection measurement issues are resolved, more testing will be done across a broader spectrum of restraint conditions to gain a more comprehensive understanding of the LODC behavior.

FUTURE EVALUATIONS

As the LODC is further refined, more test conditions will be utilized as more laboratories gain experience with the ATD. Assessments of lateral and oblique impact biofidelity, tests to evaluate the propensity of the LODC to submarine in production-representative vehicle seats with a properly positioned lap belt, and tests to evaluate the durability and instrumentation of the LODC in out-of-position tests with passenger airbags will all help to further develop the ATD. In addition, more testing is needed to assess the repeatability and reproducibility of the LODC in the various test conditions presented in this paper.

CONCLUSIONS

- NHTSA is developing a new child ATD, the Large Omnidirectional Child (LODC). The LODC has anthropometry representative of a seated child and several features such as a flexible thoracic spine, instrumented abdomen, and realistic pelvis geometry that address biofidelity and injury risk measurement concerns with the HIII-10C.
- In body region biofidelity testing, the current version of the LODC (BioRank = 1.21) displays improved biofidelity over the HIII-10C (BioRank = 2.70).
- In a test configuration similar to a previously conducted pediatric PMHS frontal test, the LODC was observed to have kinematics closer to the PMHS than the HIII-10C. Both forward and downward head trajectories were increased with the LODC consistent with PMHS behavior. Head acceleration and shoulder belt force were also more consistent with the PMHS data.
- In paired CRS tests with the HIII-10C, HIC outcomes were reduced with the LODC, indicating that chin-to-chest contact severity is mitigated by improved head kinematics and a softer thoracic structure.
- Upper and lower neck loads were on average 32.4% lower with the LODC than the HIII-10C. More study is needed to determine whether these lower loads are consistent with pediatric neck injury tolerance.
- For the chest, a second spine instrumentation location is advantageous for higher resolution restraint evaluation. However, there are issues related to chest deflection measurement in the LODC requiring more investigation.
- The presence of submarining & abdominal loading was effectively identified using a new pressure measurement method in the LODC.

ACKNOWLEDGMENTS

The authors thank the many colleagues in the injury biomechanics community who provided the pediatric biomechanical data, theses, dissertations, and any other information that was requested for this project. Without their willingness to support this work, the development of a new child ATD would not be possible. Thanks to Rakshit Ramachandra for assisting in the abdomen belt pull tests.

REFERENCES

Abdelilah Y. (2007) A Comparison of the Hybrid III Six Year-Old Dummy and Pediatric Cadaver Kinematics. *Master's thesis, University of Virginia*.

Andersson M, Bohman K, Osvalder A-L (2010) Effect of booster seat design on children's choice of seating positions during naturalistic riding. *Annu Proc Ann Adv Automot Med* 54: 181-92.

Arbogast K, Mong D, Marigowda S, Kent R, Stacey S, Mattice J, Tanji H, Higuchi K, Rouhana S (2005) Evaluating Pediatric Abdominal Injuries. *Proceedings - 19th International Technical Conference on the Enhanced Safety of Vehicles*.

Arbogast KB, Balasubramanian S, Seacrist T, Maltese MR, Garcia-Espana JF, Hopely T, Constans E, Lopez-Valdes FJ, Kent RW, Tanji H, Higuchi K (2009) Comparison of Kinematic Responses of the Head and Spine for Children and Adults in Low-Speed Frontal Sled Tests. *Stapp Car Crash Journal* 53: 329-372.

Ash J, Abdelilah Y, Crandall J, Parent D, Sherwood C, Kallieris D (2009) Comparison of Anthropomorphic Test Dummies with a Pediatric Cadaver Restrained by a Three-Point Belt in Frontal Sled Tests. *Proceedings - 21st*

International Technical Conference on the Enhanced Safety of Vehicles.

Bidez M. Burke D, King D, Mergl K, Meyer S (2007) A critical safety need for children ages 9-12 in the rear seat. *Protection of Children in Cars 5th International Conference*. Munich, Germany.

Bohman K, Arbogast K, Bostrom O (2011) Head injury causation scenarios for belted, rear-seated children in." *Traffic Inj Prev* 12(1): 62-70.

Bohman, K, Stockman, I, Jakobsson, L, Osvalder, A, Boström, O, Arbogast, K (2011) Kinematics and shoulder belt position of child rear seat passengers during vehicle maneuvers. *Ann Adv Automot Med* 55: 15-26.

Centers for Disease Control and Prevention, National Center for Health Statistics (2000) CDC growth charts: United States.

Dibb AT, Cutcliffe CC, Luck JF, Cox CA, Myers BS, Bass CR, Arbogast KB, Seacrist T, Nightingale RW (2014) Pediatric head and neck dynamics in frontal impact: Analysis of important mechanical factors and proposed neck performance corridors for 6-and 10-year-old ATDs. *Traffic Inj Prev* 15(4): 386-394.

Durbin DR, Chen I, Smith R, Elliott MR, Winston FK (2005) Effects of Seating Position and Appropriate Restraint Use on the Risk of Injury to Children in Motor Vehicle Crashes. *Pediatrics* 115(3): e305-9.

Eppinger R, Marcus J, Morgan R (1984) Development of Dummy and Injury Index for NHTSA's Thoracic Side Impact Protection Research Program. *SAE 840885*.

Forman J, Segui-Gomez M, Ash J, Lopez-Valdes F (2011) Child posture and shoulder belt fit during extended night-time traveling: an in-transit observational study. *Ann Proc Ann Adv Automot Med* 55: 3-14.

Foster CD, Hardy WN, Yang KH, King AI, Hashimoto S (2006) High-Speed Seatbelt Pretensioner Loading of the Abdomen. *Stapp Car Crash Journal* 50: 27-51.

Irwin AL, Mertz HJ (1997) Biomechanical bases for the CRABI and Hybrid III child dummies." *Stapp Car Crash Journal* 41: 261-272.

Irwin AL, Mertz HJ, Elhagediab AM, Moss S (2002) Guidelines for assessing the biofidelity of side impact dummies of various sizes and ages. *Stapp Car Crash Journal* 46: 297-319.

Jakobsson L, Bohman K, Stockman I, Andersson M, Osvalder A.-L. (2011) Older children's sitting postures when riding in the rear seat. *International Research Council on the Biomechanics of Impact*.

Kallieris D, Barz J, Schmidt G, Heess G, Mattern R (1976) Comparison Between Child Cadavers and Child Dummy by Using Child Restraint Systems in Simulated Collisions. *Stapp Car Crash Journal* 20: 511-542.

Kang YS, Bolte J, Moorhouse K, Donnelly B, Herriott R, Mallory A (2012) Biomechanical responses of PMHS in moderate-speed rear impacts and development of response targets for evaluating the internal and external biofidelity of ATDS. *Stapp Car Crash Journal* 56: 105-70.

Kang YS, Stammen JA, Moorhouse KM, Herriott R, Bolte JH (2016) PMHS Lower Neck Load Calculation using Inverse Dynamics with Cervical Spine Kinematics and Neck Mass Properties. *International Research Council on Biomechanics of Injury*.

Kent R, Lopez-Valdes F, Lamp J, Lau S, Parent D, Kerrigan J, Lessley D, Salzar R (2011) Characterization of the Pediatric Chest and Abdomen Using Three Post-Mortem Human Subjects. *Proceedings - 22nd International Technical Conference on the Enhanced Safety of Vehicles*.

Kent R, Salzar R, Kerrigan J, Parent D, Lessley D, Sochor M, Luck J, Loyd A, Song Y, Nightingale R, Bass C, Maltese M (2009) Pediatric Thoracoabdominal Biomechanics." *Stapp Car Crash Journal* 53: 373-401.

Kent R, Stacey S, Kindig M, Forman J, Woods W, Rouhana S, Higuchi K, Tanji H, St. Lawrence S, Arbogast K (2006) Biomechanical Response of the Pediatric Abdomen, Part 1: Development of an Experimental Model and Quantification of Structural Response in Dynamic Belt Loading. *Stapp Car Crash Journal* 50: 1-26.

Kent R, Stacey S, Kindig M, Woods W, Evans J, Rouhana S, Higuchi K, Tanji H, St Lawrence S, Arbogast K (2008) Biomechanical Response of the Pediatric Abdomen, Part 2: Injuries and Their

Correlation with Engineering Parameters. *Stapp Car Crash Journal* 52: 135-66.

Klinich K, Reed M, Manary M, Orton N (2010) Development and Testing of a More Realistic Pelvis for the Hybrid III 6-Year-Old ATD. *Traffic Inj Prev* 11(6): 606-12.

Klinich K, Reed M, Ritchie N, Manary M, Schneider L, Rupp J (2008) Assessing Child Belt Fit, Volume II: Effect of Restraint Configuration, Booster Seat Designs, Seating Procedure, and Belt Fit on the Dynamic Response of the Hybrid III 10YO ATD in Sled Tests. University of Michigan Transportation Research Institute Report *UMTRI-2008-49-2*.

Kremer M, Gustafson H, Bolte J, Stammen J, Donnelly B, Herriott R (2011) Pressure-Based Abdominal Injury Criteria Using Isolated Liver and Full-Body Post-Mortem Human Subject Impact Tests. *Stapp Car Crash Journal* 55: 317-350.

Lamielle S, Vezin P, Verriest JP, Petit P, Trosseille X, Vallancien G (2008) 3D Deformation and Dynamics of the Human Cadaver Abdomen under Seatbelt Loading. *Stapp Car Crash Journal* 52: 267-294.

Lemmen P, Waagmeester K, Burleigh M, Lakshminarayana A, Korschdon K, Visvikis C, Carroll J, Hynd D, Pitcher M (2013) Development of the Q10 10 Year-Old Child Crash Test Dummy. *Proceedings - 23rd International Technical Conference on the Enhanced Safety of Vehicles*.

Lopez-Valdes F, Lau A, Lamp J, Tanji H. (2010) Analysis of Spinal Motion and Loads during Frontal Impacts. Comparison between PMHS and ATD. *Assoc Adv Automot Med* 54: 61-78.

Lopez-Valdes F, Lau S, Riley P, Lamp J, Kent R (2011) The Biomechanics of the Pediatric and Adult Human Thoracic Spine. *Assoc Adv Automot Med* 55: 193-206.

Lopez-Valdes F, Seacrist T, Arbogast K, Balasubramanian S, Maltese M, Tanji H, Higuchi K, Kent R (2012) A Methodology to Estimate the Kinematics of Pediatric Occupants in Frontal Impacts. *Traffic Inj Prev* 13(4): 393-401.

Loyd A, Nightingale R, Bass C, Mertz H, Frush D, Daniel C, Lee C, Marcus J, Mukundan S, Myers B (2010) Pediatric Head Contours and Inertial Properties for ATD Design. *Stapp Car Crash Journal* 54: 167-196.

Loyd AM, Nightingale RW, Luck JF, Bass CD, Myers BS (2016) The Response of the Pediatric Heads to Impacts onto a Rigid Surface. *Journal of Biomechanics (in review)*.

Loyd A. (2009) Studies of the Human Head from Neonate to Adult: An Inertial, Geometrical and Structural Analysis. *Doctoral Dissertation, Duke University*.

Luck JF, Nightingale RW, Loyd AM, Prange MT, Dibb AT, Song Y, Fronheiser L, Myers BS (2008) Tensile Mechanical Properties of the Perinatal and Pediatric PMHS Osteoligamentous Cervical Spine. *Stapp Car Crash Journal* 52: 107-34.

Maltese MR, Castner T, Niles D, Nishisaki A, Balasubramanian S, Nysaether J, Sutton R, Nadkarni V, Arbogast KB (2008) Methods for Determining Pediatric Thoracic Force-Deflection Characteristics from Cardiopulmonary Resuscitation. *Stapp Car Crash Journal* 52: 83-105.

Mertz HJ, Jarrett K, Moss S, Salloum M, Zhao Y (2001) The Hybrid III 10-Year-Old Dummy. *Stapp Car Crash Journal* 45: 319-328.

Myers BS, McElhaney JH, Doherty BJ, Paver JG, Nightingale RW, Ladd TP, Gray L (1989) Responses of the Human Cervical Spine to Torsion. *Stapp Car Crash Journal* 33: 215-22.

NHTSA (2012a) CFR 49 Part 571, FMVSS No. 213; Child Restraints." *Final Rule*.

NHTSA (2012b) CFR 49 Part 572, Subpart T: Anthropomorphic Test Devices. *Final Rule*.

NHTSA (2015) Child Frontal Impact Sled. *NHTSA-2013-0055-0002*.

NHTSA (2005) Child passenger fatalities and injuries based on restraint use, vehicle type, seat position, and number of vehicles in the crash." *DOT HS 809784*.

NHTSA (2010) Children Injured in Motor Vehicle Traffic Crashes. *DOT HS 811 325*.

NHTSA (2005) FMVSS No. 213; Child Restraints. *Notice of Proposed Rulemaking*.

Ouyang J, Zhao W, Xu Y, Chen W, Zhong S (2006) Thoracic Impact Testing of Pediatric Cadaveric Subjects." *J Trauma* 61(6): 1492-1500.

Ouyang J, Zhu Q, Zhao W, Xu Y, Chen W, Zhong S (2005) Biomechanical Assessment of the Pediatric Cervical Spine Under Bending and Tensile Loading." *Spine* 30(24): E716-E723.

Parent DP, Crandall JR, Bolton JR, Bass CR, Ouyang J, Lau SH (2010) Comparison of Hybrid III Child Test Dummies to Pediatric PMHS in Blunt Thoracic Impact Response." *Traffic Inj Prev* 11(4): 399-410.

Parent D (2009) Scaling and Optimization of Thoracic Impact Response in Pediatric Subjects. *Master's Thesis, University of Virginia*.

Reed M, Ebert-Hamilton S, Manary M, Klinich K, Schneider L (2006) Improved Positioning Procedures for 6YO and 10YO ATDs Based on Child Occupant Postures. *Stapp Car Crash Journal* 50: 337-388.

Reed M, Sochor M, Rupp J, Klinich K, Manary M (2009) Anthropometric Specification of Child Crash Dummy Pelves through Statistical Analysis of Skeletal Geometry. *J Biomech* 42(8): 1143-5.

Rhule H, Donnelly B, Moorhouse K, Kang YS (2013) A Methodology for Generating Objective Targets for Quantitatively Assessing the Biofidelity of Crash Test Dummies. *Proceedings - 23rd International Technical Conference on the Enhanced Safety of Vehicles*.

Rhule H, Maltese M, Donnelly B, Eppinger R, Brunner J, Bolte J (2002) Development of a New Biofidelity Ranking System for Anthropometric Test Devices. *Stapp Car Crash Journal*: 46: 477-512.

Rhule H, Moorhouse K, Donnelly B, Stricklin J (2009) Comparison of WorldSID and ES-2re Biofidelity Using an Updated Biofidelity Ranking System. *Proceedings - 21st International Technical Conference on the Enhanced Safety of Vehicles*.

Seacrist T, Balasubramanian S, Garcia-Espana JF, Maltese M, Arbogast K, Lopez-Valdes F, Kent R, Tanji H, Higuchi K (2010) Kinematic Comparison of Pediatric Human Volunteers and the Hybrid III 6-Year-Old Anthropomorphic Test Device. *Annu Proc Ann Adv Automot Med* 54: 97-108.

Seacrist T, Mathews E, Balasubramanian S, Maltese M, Arbogast K (2013) Evaluation of the Hybrid III and Q-series Pediatric ATD Upper Neck Loads as Compared to Pediatric Volunteers in Low-Speed Frontal Crashes. *Ann Biomed Eng* 41(11): 2381-90.

Shaw J, Herriott R, McFadden J, Donnelly B, Bolte J (2006) Oblique and lateral impact response of the PMHS thorax." *Stapp Car Crash Journal* 50: 147-67.

Sherwood C, Shaw G, van Rooij L, Kent R, Gupta P, Crandall J, Orzechowski K, Eichelberger M, Kallieris D (2002) Prediction of Cervical Spine Injury Risk for the 6-Year-Old Child in Frontal Crashes. *Annu Proc Assoc Adv Automot Med* 46: 231-47.

Stammen J, Bolte J, Shaw J (2012) Biomechanical Impact Response of the Human Chin and Manubrium. *Ann Biomed Eng* 40(3): 666-78.

Stammen J, Donnelly B, Suntay S, Moorhouse K (2014) Dynamic Response Criteria for a Large Child ATD Thoracic Spine." *International Research Council on Biomechanics of Injury*.

Stammen J, Herriott R, Kang YS, Dupaix R, Bolte J (2012) Dynamic Properties of the Upper Thoracic Spine-Pectoral Girdle (UTS-PG) System and Corresponding Kinematics in PMHS Sled Tests. *Stapp Car Crash Journal* 56: 65-104.

Thunnissen J, Wismans J, Ewing C, Thomas D (1995) Human Volunteer Head-Neck Response in Frontal Flexion: A New Analysis. *Stapp Car Crash Journal* 39: 439-60.

van Rooij L, Harkema C, de lange R. de Jager K, Bosch-Rekveldt M, Mooi H (2005) Child poses in child restraints related to injury potential: investigations by virtual testing. *19th International Technical Conference on the Enhanced Safety of Vehicles*.

Wismans J, Maltha J, Melvin J, Stalnaker R (1979) Child Restraint Evaluation by Experimental and Mathematical Simulation. *Stapp Car Crash Journal* 23: 383-415.

Wu J, Cao L, Reed M, Hu J (2013) A Simulation Study of Spine Biofidelity in the Hybrid-III 6 Year Old ATD. *Traffic Inj Prev* 14: 397-404.

APPENDIX A: CERVICOTHORACIC TEST DETAILS

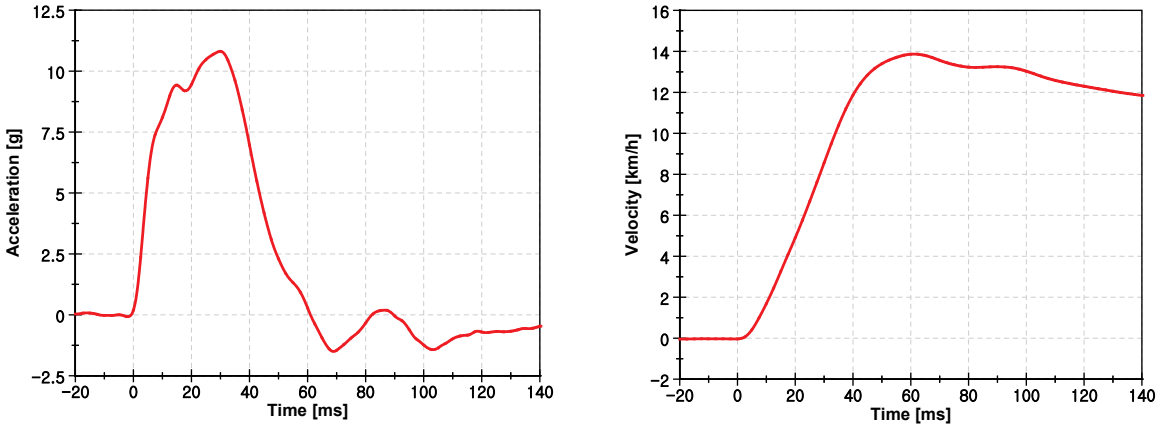

(a) acceleration (b) velocity

Figure A1. Mini-sled inputs (from Kang et al. 2016)

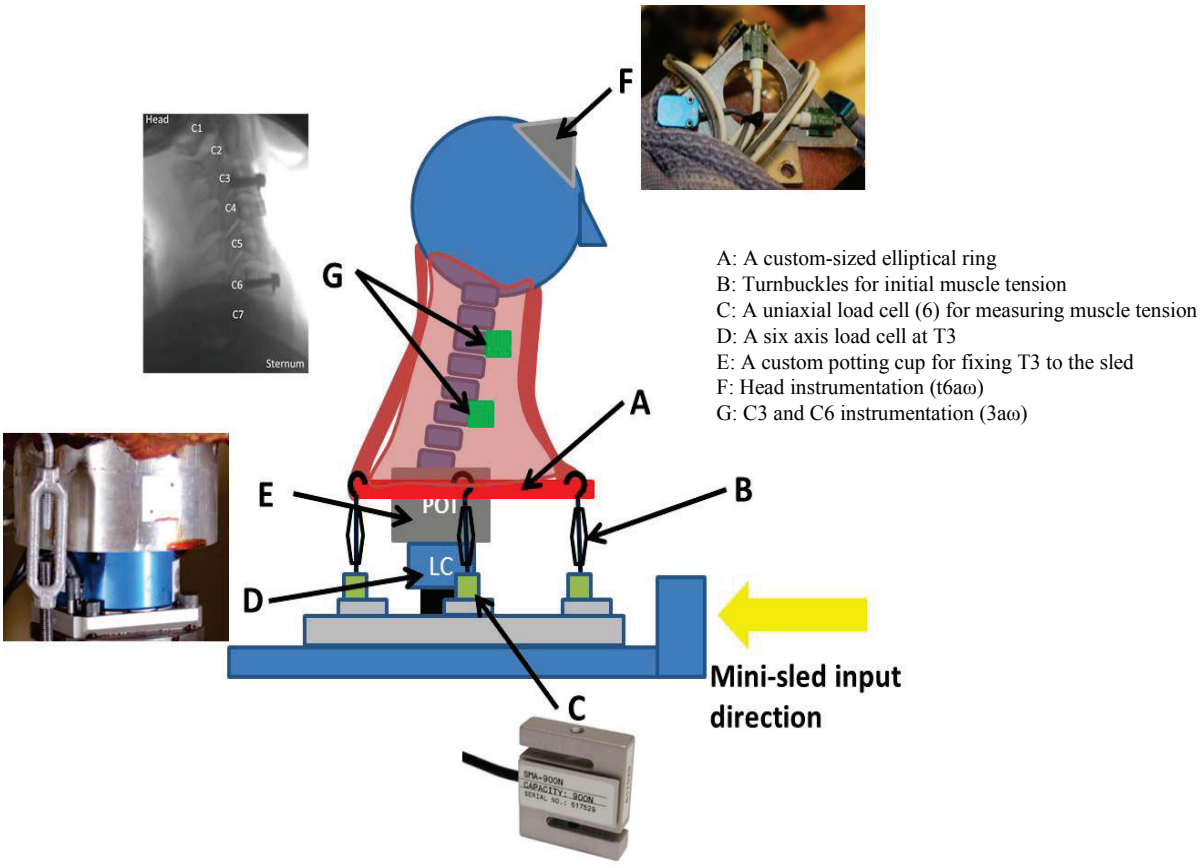

Figure A2. PMHS test setup (from Kang et al. 2016)

APPENDIX B: ATD KINEMATICS

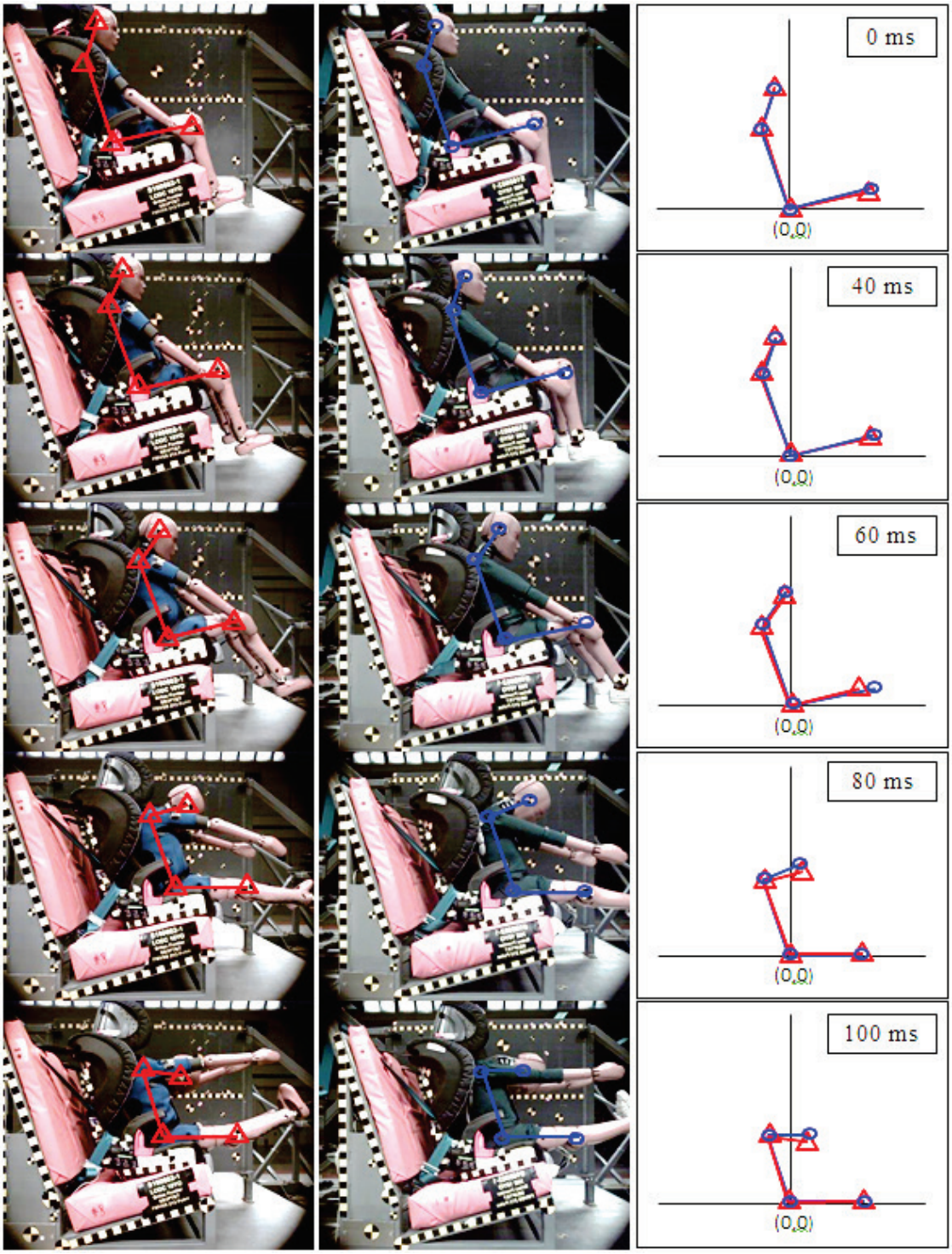

Figure B1. LODC (left) vs. HIII-10C (right) kinematics in 5 point harness test

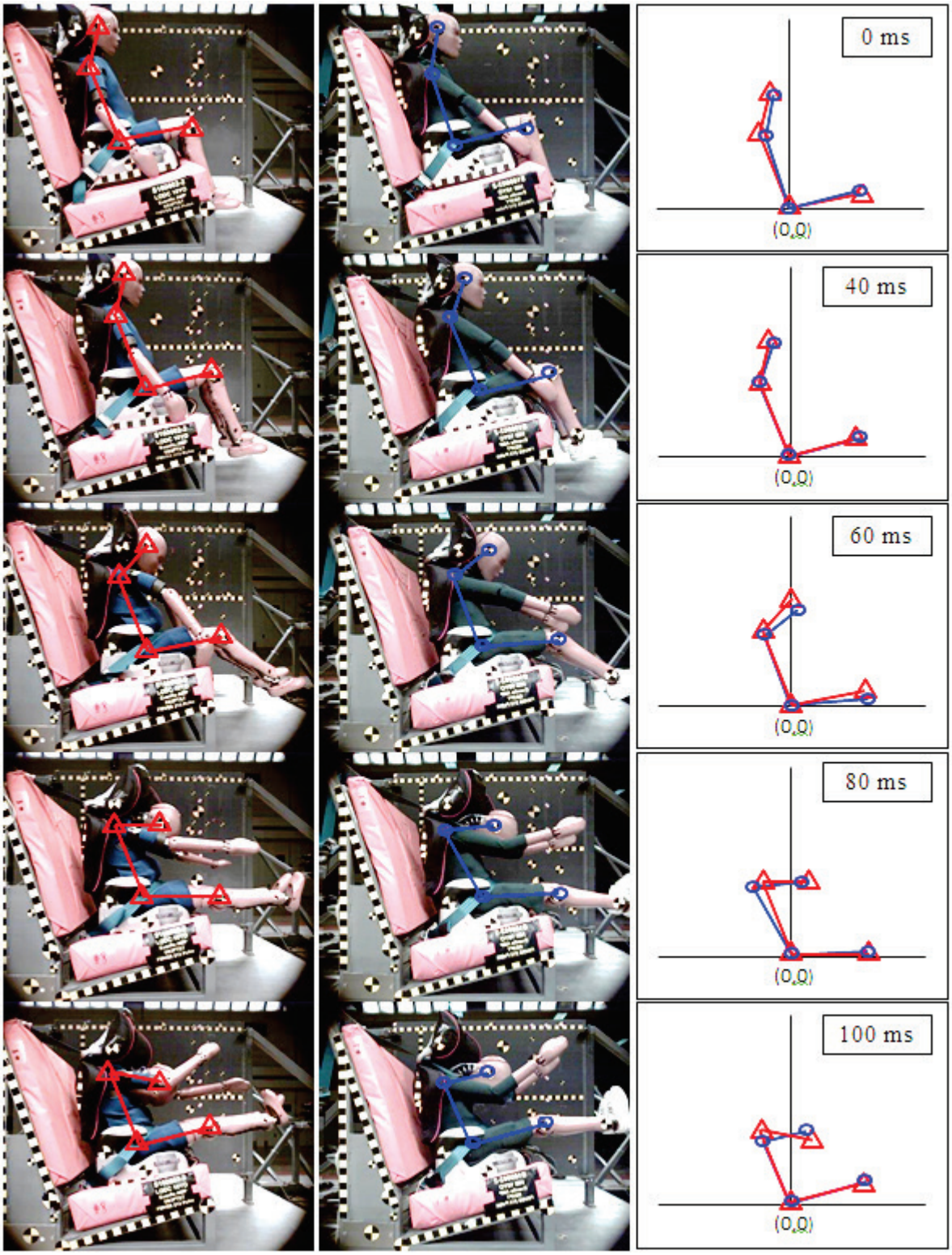

Figure B2. LODC (left) vs. HIII-10C (right) kinematics in highback booster seat test

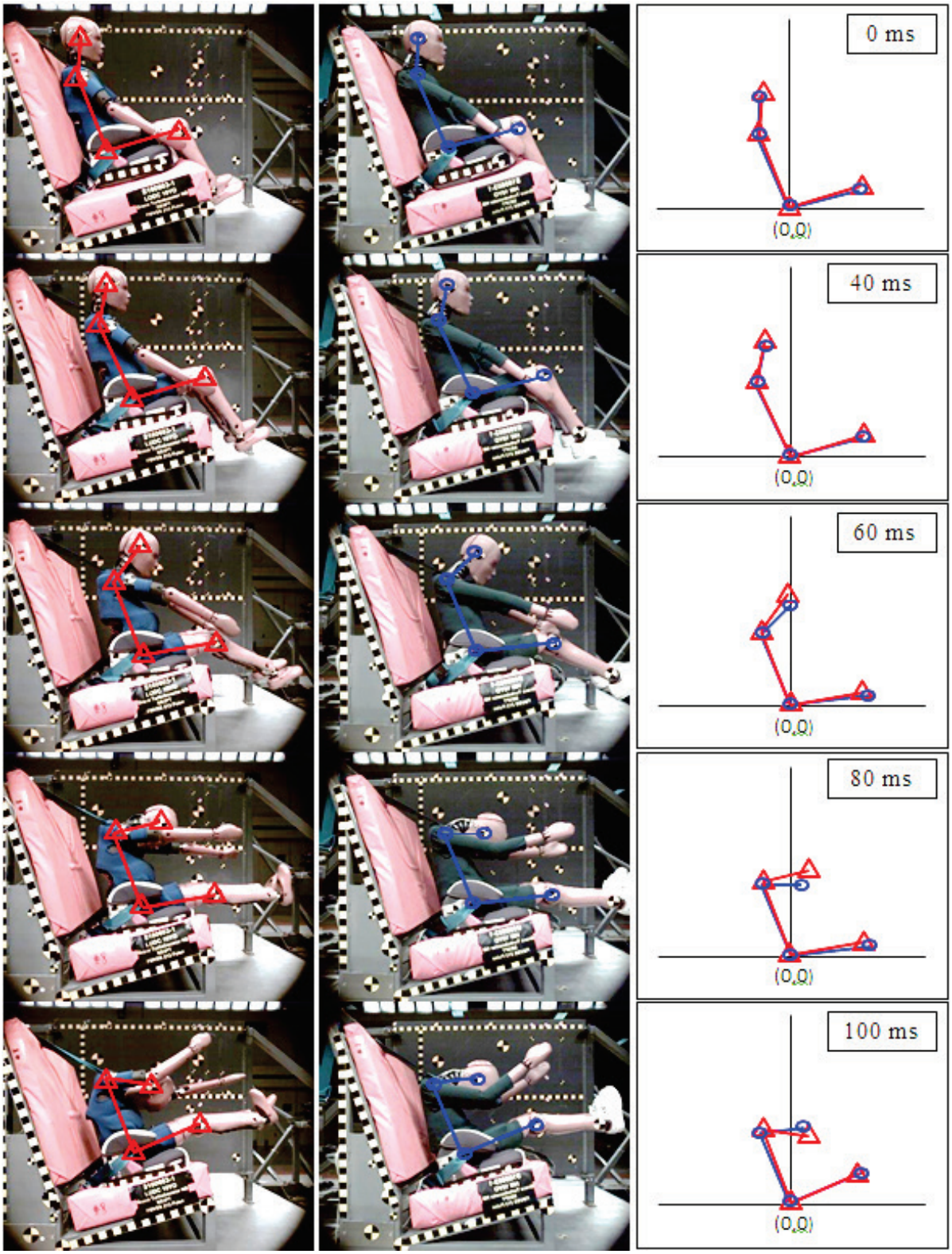

Figure B3. LODC (left) vs. HIII-10C (right) kinematics in backless booster seat test

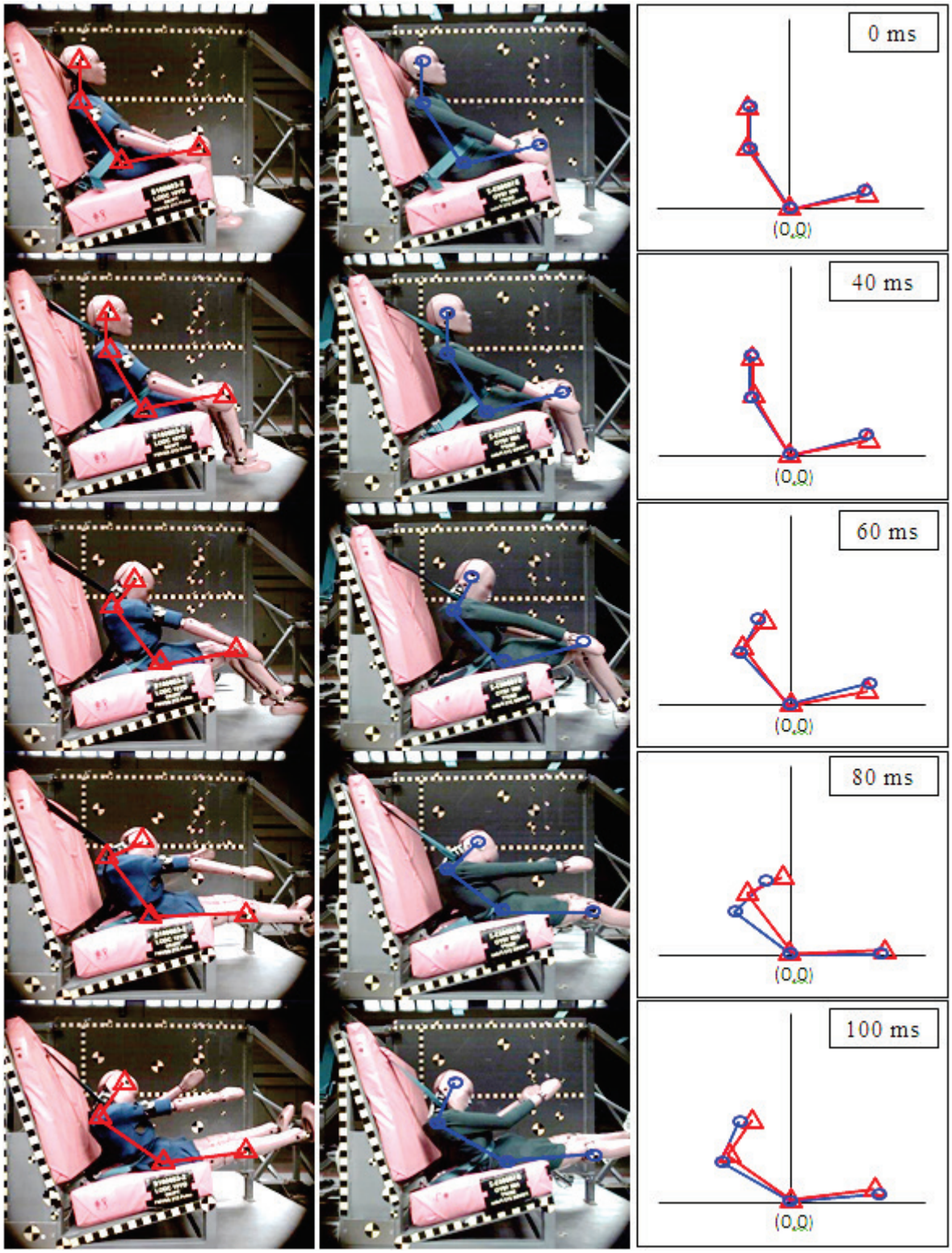

Figure B4. LODC (left) vs. HIII-10C (right) kinematics in no CRS test